Ternary System CsI-PbI_2-BiI_3 and Thermodynamic Stability of Cesium Metal Halide Perovskites

van Hattem, Andries; Alders, Dennis; Konings, Rudy J.M.; Smith, Anna L.

DOI
10.1021/acs.jpcc.3c02696

Publication date
2023

Document Version
Final published version

Published in
Journal of Physical Chemistry C

THE JOURNAL OF PHYSICAL CHEMISTRY C
A JOURNAL OF THE AMERICAN CHEMICAL SOCIETY

pubs.acs.org/JPCC
Article

Ternary System CsI–PbI_2–BiI_3 and Thermodynamic Stability of Cesium Metal Halide Perovskites

Published as part of The Journal of Physical Chemistry C virtual special issue "The Physical Chemistry of Perovskites".

Andries van Hattem, Dennis Alders, Rudy J. M. Konings, and Anna L. Smith*

Cite This: J. Phys. Chem. C 2023, 127, 17482–17496

ABSTRACT: The thermochemistry of the ternary system CsI–PbI_2–BiI_3, of interest for applications in photovoltaics, memory devices, and nuclear applications, among other things, is investigated in this work. The binary phase diagrams CsI–PbI_2 and CsI–BiI_3 were subjected to renewed experimental investigation, and the compounds $CsPbI_3$, Cs_4PbI_6, and $Cs_3Bi_2I_9$ were found to be the only stable phases in the investigated temperature window. The liquidus lines and invariant equilibria were determined. The phase equilibria in the BiI_3–PbI_2 system were measured for the first time by using Differential Scanning Calorimetry (DSC). The end-members form a solid solution over the entire composition range. The pseudobinary section $CsPbI_3$–$Cs_3Bi_2I_9$ of the CsI–PbI_2–BiI_3 ternary system was moreover measured by DSC, as well as the ternary eutectic points. A thermodynamic model of the complete CsI–PbI_2–BiI_3 system was developed by using the Compound Energy Formalism (CEF) for the solid phases and the Modified Quasichemical Model in the Quadruplet Approximation (MQMQA) for the liquid phase. The binary systems were modeled first, and no ternary interaction parameters were found necessary to reproduce accurately the phase equilibria in the ternary system. With our model, the whole liquidus surface of the field CsI–PbI_2–BiI_3 is described for the first time.

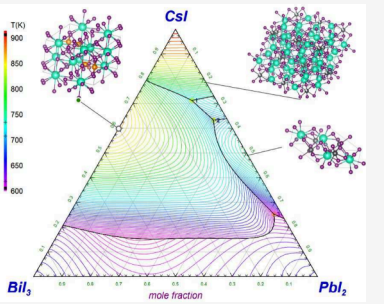

INTRODUCTION

The ternary salt system CsI–PbI_2–BiI_3, with its compounds $CsPbI_3$, Cs_4PbI_6, and $Cs_3Bi_2I_9$, is relevant for many applications, ranging from X-ray detection and scintillation purposes,[1−4] memory devices,[5−7] and LEDs[8,9] to photovoltaic solar cells.[10−13] The system is also relevant to the safety of some new types of nuclear energy generation systems. All of these applications have in common that high temperature processes are involved, so the development of thermodynamic models is extremely helpful to describe synthesis and operating conditions of the envisaged materials.

One of the reasons for the high interest is the fact that the halide perovskite phases that occur in the CsI–PbI_2–BiI_3 system have favorable optoelectronic properties. They are applied in a variety of forms in devices, thin films, nanocrystalline materials, or single crystals. The latter, used in X-ray detection and scintillation techniques, are grown from the molten state by the Czochralski or Bridgman methods using slow pulling and cooling. This is a quasi-equilibrium process, governed by kinetics and thermodynamics. Thin films are generally produced by physical or chemical vapor deposition (respectively, PVD and CVD),[14,15] in which the crystalline layers are deposited on a substrate from a vapor phase composed of the individual precursors. Although it is a nonequilibrium process, chemical thermodynamic considerations are highly useful in predicting the stable materials at the temperature, (gas) pressure, and concentrations in a CVD reactor.

A lesser known application is in the area of safety assessment of the lead-cooled fast reactor (LFR), a type of nuclear reactor selected by the Generation IV International Forum as a potential candidate for the future of nuclear energy.[16−24] Features that make the LFR an attractive candidate are the use of a fast-neutron spectrum and the possibility of operating in a closed fuel cycle, allowing for actinide recycling. In this type of nuclear reactor, either liquid lead (Pb) or lead–bismuth eutectic (LBE) is used as a coolant. For the safety assessment of the LFR, it is important to know how these coolants will interact with radiotoxic and volatile fission products such as cesium (Cs) and iodine (I) in case the cladding around a nuclear fuel pin would break.[25,26] Because of the very high temperature and thermal gradient inside a mixed oxide $(U,Pu)O_2$ fuel pellet, volatile fission products like Cs and I tend to migrate to the periphery of the fuel pin,[25,27] meaning

Received: April 24, 2023
Revised: July 6, 2023
Published: August 28, 2023

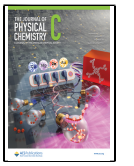

https://doi.org/10.1021/acs.jpcc.3c02696
J. Phys. Chem. C 2023, 127, 17482–17496

they will be among the most likely elements to come in contact with the coolant upon clad breach.

Knowledge of the equilibrium phase diagrams in the CsI−PbI_2−BiI_3 system is very limited, and the available data are not recent. CsI−PbI_2 and CsI−BiI_3 were investigated for the last time in 1972 and 1988, respectively. To the best of our knowledge, no phase diagrams of the binary BiI_3−PbI_2 or the ternary CsI−PbI_2−BiI_3 systems were ever reported in literature. For that reason we have made a systematic study of this system, with experimental investigations of the binary systems, of selected compositions in the ternary system, and a CALPHAD-base assessment, to provide a sound chemical thermodynamic description of the phase equilibria in the ternary system.

Three phase diagram investigations into the CsI−BiI_3 system were found in literature: a study from Plyushev et al. from 1970,[28] a study from Dzeranova et al. from 1984,[29] and a study from Kun et al. from 1988.[30] The three phase diagrams agree on the fact that there is only one compound that forms eutectic systems with the end members CsI and BiI_3. However, there is some confusion about the exact composition of the compound: Plyuschev et al. report it as $Cs_3Bi_2I_9$, while Dzeranova et al. report it to be "Cs_3BiI_6", with the strange remark that this compound corresponds to 57% CsI. Kun et al. later report $Cs_3Bi_2I_9$. Upon analysis of the *d*-spacing that is reported for "Cs_3BiI_6" by Dzeranova et al., we consider it to be actually a mixture of CsI and $Cs_3Bi_2I_9$. This observation undermines the paper by Kaloev et al.[31] that analyses the phase diagram based on the wrong composition. Kun et al. report moreover a homogeneity range up to 4.7 mol % for $Cs_3Bi_2I_9$, hence $Cs_3Bi_2I_9$ is actually the nonstoichiometric compound $Cs_{3-x}Bi_{2+x}I_{9+2x}$, with x either positive or negative. To increase the legibility in and of this work, however, the notation $Cs_3Bi_2I_9$ will be used for this nonstoichiometric compound. The data points reported in refs 28−30 are reproduced in the phase diagram optimization, see Figure 6. The melting temperature of $Cs_3Bi_2I_9$ reported in refs 28 and 30 is also listed in Tables 6 and 7. The crystal structure of $Cs_3Bi_2I_9$ was already elucidated in 1968 by Lindqvist.[32] More recently, it was found by Johansson et al. that between $Cs_3Bi_2I_9$ and BiI_3, only mixtures of these two compounds are formed.[13] When assessing other claims, it is necessary to clearly discriminate between compounds that form as bulk powder and, e.g., thin films. In studies on thin films, e.g., reports on $CsBi_3I_{10}$ are found,[12] though it also claimed to form as freestanding material.[33] The latter authors propose a degradation mechanism in which the decomposition temperature of $CsBi_3I_{10}$ would be 428 K. Polymorphism for $Cs_3Bi_2I_9$ was investigated below room temperature.[34−37] Kun et al.[30] claim a transition to a high-temperature polymorph of $Cs_3Bi_2I_9$ at 605 K; to the best of our knowledge, they are the only ones.

In the phase diagram optimization, the congruent melting point of $Cs_3Bi_2I_9$ was derived to be 874 K (*vide infra*). However, thermal degradation of a single crystal was reported to occur already at 823 K.[4] Thermogravimetric analysis (TGA) measurements of $Cs_3Bi_2I_9$ by Gu et al. report a large weight loss at 698 K and another at 923 K.[38] Thermal expansion of $Cs_3Bi_2I_9$ was determined using in situ synchrotron X-ray diffraction by McCall et al. in 2017.[39] The authors measured the X-ray diffraction patterns starting at 298 and up to 873 K with intervals of 6−10 K. They report Bragg peaks to remain from room temperature to decomposition at 775 K, after which $Cs_3Bi_2I_9$ starts to dissociate. A discontinuity in the lattice parameter is observed at 682 K. In their differential thermal analysis (DTA), they observe events at 815 K, which they assigned to BiI_3 boiling, and at 883 K, which they state to nearly coincide with the melting of CsI (905 K). This interpretation does not agree with dedicated phase diagram investigations.

Regarding thermodynamic data on the ternary compound, the melting enthalpy was measured by Kun et al.[30] They found the value of (148 ± 2.2) kJ·mol^{-1} at T = (905 ± 5) K. To the best of our knowledge, no experimental data on the enthalpy of formation, entropy, or heat capacity at $T \geq 300$ K of $Cs_3Bi_2I_9$ are available in the literature. A recent experimental measurement[40] of the low temperature heat capacity of $Cs_3Bi_2I_9$ is not in agreement with our measurements (unpublished results). A computational study reports the enthalpy of formation of $Cs_3Bi_2I_9$ at 0 K to be −1345 kJ·mol^{-1}.[41]

Two phase diagram investigations were performed for the system CsI−PbI_2. First, the liquidus line was published by Ilyasov et al. in 1967.[42] They reported that Cs_4PbI_6 melts with peritectic decomposition and $CsPbI_3$ to melt congruently. Second, a complete phase diagram was published in 1969 by Belyaev et al.[43] The data points reported by[42,43] are reproduced in the phase diagram optimization in Figure 7. The two intermediate compounds are well-established in the scientific literature: $CsPbI_3$ since 1893[44] and Cs_4PbI_6 since 1960.[45] Several polymorphs of $CsPbI_3$ exist, but the stable states are limited to δ-$CsPbI_3$ at room temperature and α-$CsPbI_3$ at high temperature until melting.

Thermodynamic data are mostly limited to the study of enthalpic properties in $CsPbI_3$: the enthalpies of formation and transition were studied several times. Wang et al. measured the enthalpy of formation from binary iodides using solution calorimetry with DMSO as solvent.[46,47] Tsvetkov et al. also used solution calorimetry with a DMSO−water mixture as solvent.[48] Sereda et al.[49] derived the enthalpy of reaction from the iodides using high temperature heat flux inverse drop calorimetry. They found within error the same value, although the error is much larger than that reported by the other publications. The results are in excellent agreement, as shown in Table 1. The enthalpy of the phase transition in $CsPbI_3$ was studied by Dastidar et al.[50] and by Wang et al.[46] Their results are included in Table 6. Using DFT, Kye et al. also found α-$CsPbI_3$ to have a negative enthalpy of formation, though it was less negative than δ-$CsPbI_3$, i.e., the α-polymorph is only metastable with respect to the δ-phase.[51] The low temperature heat capacity of $CsPbI_3$ was only reported from 0.4 up to 150 K by Evarestov et al.[52]

Table 1. Reported Experimentally Determined Enthalpy of Formation of δ-$CsPbI_3$

$\Delta_f H°$ (298.15 K)/kJ·mol^{-1}	method	ref
−539.0 ± 0.9	solution calorimetry	46
−539.1 ± 0.4	solution calorimetry	48
−537.5 ± 6.0	drop calorimetry	49

As a sidenote, the Cs_2PbX_4 and $CsPb_2X_5$ compounds, which were studied using time-dependent density functional theory (TD-DFT), do not exist as bulk compounds for X = I,[53] though there can be two-dimensional materials formed via nonambient pressure routes.[54]

Compared to the two systems discussed in *supra*, practically nothing is known about the BiI_3−PbI_2 system. No compounds

https://doi.org/10.1021/acs.jpcc.3c02696
J. Phys. Chem. C 2023, 127, 17482−17496

have been reported. To the best of our knowledge, no phase diagram was ever reported on this system, neither is any thermodynamic property known. The phases that occur in the system have not been identified clearly. In 1999, a paper describing the $(PbI_2)_x-(BiI_3)_{1-x}$ structure was reported, but the study is inconclusive with respect to the solid solution phases, their structural ordering, and their thermal stability.[55] From an application point of view, a study by Neuhausen and Eichler from 2006 on the thermal release of iodine from liquid eutectic lead bismuth alloy is of interest.[56] Although this study is important in the practical assessment of the evaporation of radioiodine, it does not explain the nature of the solid behavior of mixtures of PbI_2 and BiI_3 at the atomic scale. A single DSC measurement at $x = 0.50$ is known, reporting a single thermal event at 654 K.[7] Alexander et al. studied the structure of this system at a composition $x_{BiI_3} = 0.5$[6] using, among other techniques, single-crystal XRD, transmission electron microscopy (TEM), scanning electron microscopy with energy dispersive scattering (SEM/EDS), and powder XRD. Their XRD and EDS data indicate that Pb^{2+}, Bi^{3+}, and vacancies share the same site, while iodine has a fully occupied position. The TEM and electron diffraction data indicate microstructured composites with two phases with mixed occupancies.

No complete thermodynamic investigations into the ternary phase diagram are known to us. Bismuth doping into $CsPbI_3$ was studied, however. Papers on $CsPb_{1-x}Bi_xI_3$ can be interpreted as a study of the subsolidus field of the section $CsPbI_3$–"$CsBiI_4$". In 2017, Hu and co-workers[10] investigated the bismuth incorporation into α-$CsPbI_3$. Initially, this stabilizes the α-polymorph. According to the authors, above 10% bismuth incorporation, the δ-polymorph is again the most stable crystal structure at room temperature. Computational research using DFT by Zhang et al. contradicts the attribution of this effect to incorporation of Bi^{3+}, though stating that incorporation of Bi(0) would stabilize the high temperature structure.[57] In a following publication, Zhang et al. state that the perovskite stabilizing due to the B-site doping is only valid for Sn^{2+}-doping. The authors claim that if the effect is found experimentally, this depends probably on the synthesis route and it is not due to the inherent physics of $CsPb_{1-x}Bi_xI_3$.[58] Kye et al. found similar results.[51] For thin films, the metastability of α-$CsPbI_3$ with respect to δ-$CsPbI_3$ upon Bi^{3+}-doping was also experimentally proven: above 393 K, the films turn into the δ-$CsPbI_3$ variant.[59]

METHODS

Synthesis. The chemicals CsI (Merck, 99.999%), PbI_2 (Merck, 99.999%), and BiI_3 (Alfa Aesar, 99.998%) were purchased. All samples were handled inside an Ar-filled glovebox with low oxygen and water content (<5 ppm) and not exposed to air in any stage of the experiments. $CsPbI_3$ was synthesized by mixing CsI and PbI_2 in a 1:1 ratio. The mixture was ground and heated to the melt (823 K) in a nickel liner in an airtight stainless steel container. It was kept for 30 min in the melt, after which it was cooled down to 723 K. This temperature was maintained for 1 h. Cs_4PbI_6 was synthesized via a solid state reaction. CsI and PbI_2 were mixed in a 4:1 ratio, ground, and put in a nickel liner in an airtight stainless steel container. It was heated to 673 K for 48 h. $Cs_3Bi_2I_9$ was synthesized by mixing CsI and BiI_3 in a 3:2 ratio, thoroughly grinding, and heating twice in the aforementioned containment for 12 h at 723 K with intermittent regrinding.

X-ray Diffraction. Formation and purity of the compounds were confirmed by powder X-ray diffraction (XRD), using a PANalytical X'Pert PRO X-ray diffractometer mounted in the Bragg–Brentano configuration with a Cu-anode (0.4 mm by 12 mm line focus, 45 kV, 40 mA). The data were collected using an X'celerator detector in the angle range $10° \leq 2\theta \leq 120°$, with 0.008° 2θ increments. The total measurement time was about 7 h. Inside the argon-filled glovebox, the samples were loaded in airtight sample holders closed with Kapton foil to prevent reaction with moisture from the atmosphere. Structural analysis was performed on the diffraction patterns using the profile refinement method[60,61] or LeBail method[62] in the FullProf suite.[63]

Differential Scanning Calorimetry. Phase diagram measurements were performed using differential scanning calorimetry (DSC) on a Setaram Multi-Detector HTC Module of the 96 Line calorimeter with 3D heat flux detection. The temperature on the heating ramp was calibrated by measuring the melting points of standard high purity metals (In, Sn, Pb, Al, Ag, Au). The calibration was performed as recommended in ref 64. Typically, CsI, PbI_2, and BiI_3 and their binary and ternary mixtures were measured. Samples were prepared inside the glovebox under purified Ar-atmosphere, in which the powders were mixed and loaded in closed stainless steel containers with liners made of nickel.[65] The samples were heated under an argon flow in the DSC apparatus with a heating rate of 10 K/min to complete melting to ensure complete mixing. Subsequently, 4 cycles with heating at 10 K/min and cooling at various rates were performed to obtain equilibrium data. For several samples, the liners were opened after the measurements and the samples were analyzed using XRD. Besides these mixtures, measurements for synthesized Cs_4PbI_6 and $Cs_3Bi_2I_9$ were performed too. The melting point, decomposition temperature, and polymorphic and eutectic phase transition temperatures are based on the determination of the onset temperature of the recorded heat flow event on heating. The estimated uncertainties are ±5 K for pure compounds and ±10 K for mixtures. The liquidus events are based on the peak maximum of the last event collected on the heating ramp.[66] The estimated uncertainty is ±10 K. The data collected on cooling were not used for the determination of phase equilibria but rather to check the number of invariant reactions occurring for a given composition.

Thermodynamic Modeling. The thermodynamic modeling of the binaries CsI–PbI_2, CsI–BiI_3, and BiI_3–PbI_2, as well as the ternary system CsI–PbI_2–BiI_3, was performed based on the CALPHAD (CALculation of PHase Diagrams) method[67] using the FactSage software, version 8.2.[68] Experimental data obtained in this work were used in combination with data reported in the literature as a basis for optimization of the excess Gibbs energy functions of the salt systems of interest.

Stoichiometric Compounds. The Gibbs energy function for the stoichiometric compounds CsI, PbI_2, BiI_3, $CsPbI_3$, Cs_4PbI_6, and $Cs_3Bi_2I_9$ is given by

$$G^{\varphi}(T) - \Sigma_i n_i^{\varphi} H_i^{\mathrm{SER}}\ (298.15\ \mathrm{K}) = a + bT + cT\ln T + \Sigma d_n T^n \quad (1)$$

where n_i^{φ} is the number of atoms in the ith element in the formula; n is an integer (2, 3, −1, ...); a, b, c, and d_n are optimized coefficients of the Gibbs energy function related to

https://doi.org/10.1021/acs.jpcc.3c02696
J. Phys. Chem. C 2023, 127, 17482−17496

Table 2. Thermodynamic Functions Used in the CALPHAD Model in This Work[a]

compound	$\Delta_f H^\circ_m$(298.15 K) (kJ·mol^{-1})	S°_m(298.15 K) (J·K^{-1}·mol^{-1})	$C_{p,m}(T)$ (J·K^{-1}·mol^{-1}) = $A + BT + CT^{-2} + DT^2$				temp range (K)	source
			A	B	C	D		
CsI(s)	−348.100	122.2	43.815	0.0218422	200247.7	2.495766×10^{-6}	[298−905]	69
CsI(l)	−331.9116	131.90	74.268				[905−1500]	69
PbI_2(s)	−175.3933	174.837	114.6362	−0.12982	−942533.9	1.377482×10^{-4}	[298−683]	70
PbI_2(l)	−162.5087	185.92	108.5748				[683−1500]	70,71
BiI_3(s)	−150.624	224.681	40.95	0.1086732	288972.0	-3.519×10^{-8}	[298−682]	72,73
BiI_3(l)	−127.7018	246.17	150.624				[682−1000]	74
δ-$CsPbI_3$	**−543.000**	**294.8**	158.4512	−0.10798	−742286	1.4×10^{-4}	[298−594]	this work[46,48]
α-$CsPbI_3$	**−528.800**	**318.706**	158.4512	−0.10798	−742286	1.4×10^{-4}	[594−763]	this work[50]
Cs_4PbI_6	**−1598.000**	**658.3**	289.8962	−0.04246	−141543	1.48×10^{-4}	[298−764]	this work
$Cs_3Bi_2I_9$	**−1478.243**	**819.2**	211.365	0.285606	600749	7.49×10^{-6}	[298−905]	this work

[a]The heat capacity is expressed as the following polynomial: $C_{p,m}(T) = A + BT + CT^{-2} + DT^2$. Optimized values are marked in **bold**.

the values of the enthalpy of formation, standard entropy, and heat capacity.

The thermodynamic functions selected in this work to describe the end-members and intermediate compounds are listed in Table 2. The thermodynamic functions for CsI are taken from Capelli et al.[69] For PbI_2(s), the enthalpy of formation and entropy are taken from JANAF.[70] A fit for the heat capacity of the solid phase was made to the heat capacity values listed by JANAF.[70] The enthalpy of transition (PbI_2(s) = PbI_2(l)), as reported by Konings et al.[71] (23.5 kJ·mol^{-1}), is used, which is close to the value reported in JANAF (23.4 kJ·mol^{-1}). The heat capacity for the liquid phase is also taken from JANAF.[70] The standard enthalpy of formation and entropy of BiI_3(s) are taken from Cubicciotti.[72] The heat capacity for the solid phase and enthalpy of melting are taken from Barin et al.[73] The heat capacity for BiI_3(l) is taken from Cubiccioti and Eding.[74] The enthalpy of formation of δ-$CsPbI_3$ is based on the measurements of Wang et al. and Tsvetkov et al.[46,48] The standard enthalpy of formation and entropy of α-$CsPbI_3$ are correlated to those of δ-$CsPbI_3$ via the enthalpy of the phase transition, as measured by Dastidar et al.[50] and Wang et al.[46] The standard entropy of δ-$CsPbI_3$ was optimized in this work, as well as the standard enthalpy of formation and entropy of Cs_4PbI_6 and $Cs_3Bi_2I_9$. The heat capacities of $CsPbI_3$, Cs_4PbI_6, and $Cs_3Bi_2I_9$ were estimated using the Neumann−Kopp rule.[75,76]

Liquid Solution. The excess Gibbs energy terms of the liquid solutions are modeled using the quasi-chemical formalism in the quadruplet approximation, as proposed by Pelton et al.[77] This method is well-suited to the modeling of chloride and fluoride molten salt systems and was applied herein to a new class of halide salts, namely, iodide salts. In the liquid phase, the lead and bismuth cations are taken to be symmetric with respect to each other, whereas the monovalent Cs are taken to be asymmetric.

This description of the melt assumes the existence of quadruplets in the liquid, allowing for the incorporation of short-range ordering into the thermodynamic model. A schematic depiction of a quadruplet is given in Figure 1. This formalism allows for the selection of the composition of maximum short-range ordering, often found at the lowest eutectic or congruent melting point of an intermediate, through the choice of cation−cation coordination numbers. The anion−anion coordination numbers are subsequently fixed through the electroneutrality rule. The coordination numbers used in this work are given in Table 3.

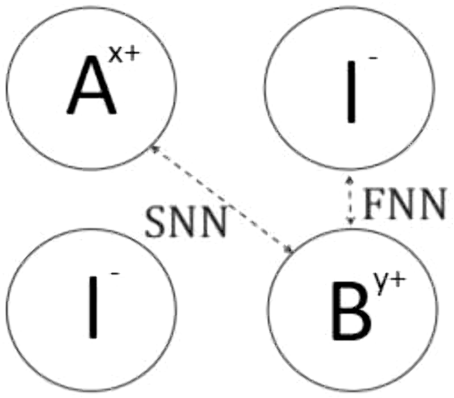

Figure 1. Schematic representation of a quadruplet used in the quadruplet approximation. In this figure, A^{x+} and B^{y+} are the cations in a system, while I^- is the anion. The first-nearest neighbor (FNN) and second-nearest neighbor (SNN) are also shown.

Table 3. Coordination Numbers Used in the CALPHAD Models Presented in This Work

A^{x+}	B^{y+}	Z^A_{AB/I_2}	Z^B_{AB/I_2}	Z^I_{AB/I_2}
Cs^+	Cs^+	6	6	6
Pb^{2+}	Pb^{2+}	6	6	3
Bi^{3+}	Bi^{3+}	6	6	2
Cs^+	Pb^{2+}	6	6	4
Cs^+	Bi^{3+}	3	6	2.4
Pb^{2+}	Bi^{3+}	6	6	2.4

The change in energy associated with the second-nearest neighbor exchange reaction, given in eq 2 for the system CsI−PbI_2, is given in eq 3. This excess Gibbs energy parameter is one of the optimization parameters used in this work.

$$(Cs{-}I{-}Cs) + (Pb{-}I{-}Pb) \rightarrow 2(Cs{-}I{-}Pb)\Delta g_{CsPb/I_2} \quad (2)$$

$$\Delta g_{CsPb/I_2} = \Delta g^0_{CsPb/I_2} + \Sigma_{i\geq 1} g^{i0}_{CsPb/I_2} \chi^i_{CsPb/I_2} + \Sigma_{j\geq 1} g^{0j}_{CsPb/I_2} \chi^j_{PbCs/I_2} \quad (3)$$

In eq 3 the terms $\Delta g^0_{CsPb/I_2}$, g^{i0}_{CsPb/I_2} and g^{0j}_{PbCs/I_2} are composition-independent coefficients that may depend on temperature. The composition dependence of the Gibbs energy is apparent

https://doi.org/10.1021/acs.jpcc.3c02696
J. Phys. Chem. C 2023, 127, 17482−17496

Table 4. Summary of the Thermodynamic Data Used in the Present Work to Model the Solid Phases of the CsI−PbI_2−BiI_3 System[a]

phase	Gibbs energy (J·mol^{-1})	source
solid solution	${}^{\circ}G_{(Bi^{3+})_1(I^-)_2} - 2{}^{\circ}H_I^{SER} - {}^{\circ}H_{Bi}^{SER} = {}^{\circ}G_{BiI_3} - {}^{\circ}G_I^{SER} + 7.9384T - 50000$	this work
$(Cs^+,Pb^{2+},Bi^{3+},Va)_1(I^-,Va)_2$	${}^{\circ}G_{(Bi^{3+})_1(Va)_2} - {}^{\circ}H_{Bi}^{SER} = {}^{\circ}G_{BiI_3} - 3{}^{\circ}G_I^{SER} + 7.9384T - 50000$	this work
	${}^{\circ}G_{(Pb^{2+})_1(I^-)_2} - 2{}^{\circ}H_I^{SER} - {}^{\circ}H_{Pb}^{SER} = {}^{\circ}G_{PbI_2}$	this work
	${}^{\circ}G_{(Pb^{2+})_1(Va)_2} - {}^{\circ}H_{Pb}^{SER} = {}^{\circ}G_{PbI_2} - 2{}^{\circ}G_I^{SER}$	this work
	${}^{\circ}G_{(Cs^+)_1(Va)_2} - 3{}^{\circ}H_{Cs}^{SER} = {}^{\circ}G_{CsI} - {}^{\circ}G_I^{SER} + 11.5263T$	this work
	${}^{\circ}G_{(Cs^+)_1(I^-)_2} - 2{}^{\circ}H_I^{SER} - {}^{\circ}H_{Cs}^{SER} = {}^{\circ}G_{CsI} + {}^{\circ}G_I^{SER} + 11.5263T$	this work
	${}^{\circ}G_{(Va)_1(I^-)_2} - 2{}^{\circ}H_I^{SER} = 2{}^{\circ}G_I^{SER} + \mathbf{100000}$	this work
	${}^{\circ}G_{(Va)_1(Va)_2} = \mathbf{100000}$	this work
	${}^{0}L_{(Pb^{2+},Bi^{3+})_1(I^-)_2} = \mathbf{2500}$	this work
	${}^{0}L_{(Pb^{2+},Va)_1(I^-)_2} = \mathbf{-3000}$	this work
	${}^{0}L_{(Bi^{3+},Cs^+)_1(I^-)_2} = \mathbf{100000}$	this work
	${}^{0}L_{(Cs^+,Pb^{2+})_1(I^-)_2} = \mathbf{60000}$	this work
	${}^{0}L_{(Cs^+,Pb^{2+})_1(Va)_2} = \mathbf{60000}$	this work
homogeneity range	${}^{\circ}G_{(Cs^+)_3(Bi^{3+})_2(I^-)_9} - 3{}^{\circ}H_{Cs}^{SER} - 2{}^{\circ}H_{Bi}^{SER} - 9{}^{\circ}H_I^{SER} = {}^{\circ}G_{Cs_3Bi_2I_9}$	this work
$(Cs^+,Va)_3(Bi^{3+},Va)_2(I^-,Va)_9$	${}^{\circ}G_{(Cs^+)_3(Bi^{3+})_2(Va)_9} - 3{}^{\circ}H_{Cs}^{SER} - 2{}^{\circ}H_{Bi}^{SER} = {}^{\circ}G_{Cs_3Bi_2I_9} - 9{}^{\circ}G_I^{SER}$	this work
	${}^{\circ}G_{(Cs^+)3(Va)2(I^-)_9} - 3{}^{\circ}H_{Cs}^{SER} - 9{}^{\circ}H_I^{SER} = 3{}^{\circ}G_{CsI} + 6{}^{\circ}G_I^{SER} + 47.6278T$	this work
	${}^{\circ}G_{(Cs^+)_3(Va)_2(Va)_9} - 3{}^{\circ}H_{Cs}^{SER} = 3{}^{\circ}G_{CsI} - 3{}^{\circ}G_I^{SER} + 47.6278T$	this work
	${}^{\circ}G_{(Va)_3(Bi^{3+})_2(I^-)_9} - 2{}^{\circ}H_{Bi}^{SER} - 9{}^{\circ}H_I^{SER} = 2{}^{\circ}G_{BiI_3} + 3{}^{\circ}G_I^{SER} + 47.6278T$	this work
	${}^{\circ}G_{(Va)_3(Bi^{3+})_2(Va)_9} - 2{}^{\circ}H_{Bi}^{SER} = 2{}^{\circ}G_{BiI_3} - 6{}^{\circ}G_I^{SER} + 47.6278T$	this work
	${}^{\circ}G_{(Va)_3(Va)_2(I^-)_9} - 9{}^{\circ}H_I^{SER} = 9{}^{\circ}G_I^{SER} + {}^{\circ}G_{(Va)_3(Va)_2(Va)_9}$	this work
	${}^{\circ}G_{(Va)_3(Va)_2(Va)_9} = \mathbf{100000}$	this work
	${}^{0}L_{(Cs^+)_3(Va)_2(I^-,Va)_9} = \mathbf{200000}$	this work
	${}^{1}L_{(Cs^+)_3(Va)_2(I^-,Va)_9} = \mathbf{120000}$	this work
	${}^{0}L_{(Va)_3(Bi^{3+})_2(I^-,Va)_9} = \mathbf{100000}$	this work
	${}^{1}L_{(Va)_3(Bi^{3+})_2(I^-,Va)_9} = \mathbf{150000}$	this work
	${}^{0}L_{(Cs^+,Va)_3(Bi^{3+})_2(I^-)_9} = \mathbf{70000}$	this work
	${}^{0}L_{(Cs^+)_3(Bi^{3+},Va)_2(I^-)_9} = \mathbf{110000}$	this work
functions	${}^{\circ}G_I^{SER} = 100565.721 - 41.4565742T - 20.78611T \ln T$ $(298 < T < 900\ K)$	70
	${}^{\circ}G_I^{SER} = 100490.766 - 39.9796783T - 21.02293T \ln T - 0.00028892195T^2 - 5.92257 \times 10^{-8}T^3 + 4271.7805T^{-1}$ $(900 < T < 2400\ K)$	70
	${}^{\circ}G_{BiI_3} = -157970.93 + 65.731T - 40.95T \ln T - 0.0543366T^2 + 5.865 \times 10^{-9}T^3 - 1444860T^{-1}$ $(298 < T < 681.8\ K)$	72,73
	${}^{\circ}G_{PbI_2} = -208180.225 + 565.688T - 114.6362T \ln T + 0.06491T^2 - 2.2958 \times 10^{-5}T^3 + 471266.95T^{-1}$ $(298 < T < 683\ K)$	70
	${}^{\circ}G_{CsI} = -361484.671 + 176.752T - 43.815T \ln T - 0.0109211T^2 - 4.15961 \times 10^{-7}T^3 - 100123.85T^{-1}$ $(298 < T < 905\ K)$	69
	${}^{\circ}G_{\delta\text{-}CsPbI_3} = -589169.342 + 744.645685T - 158.4512T \ln T + 0.05399T^2 - 2.3333 \times 10^{-5}T^3 + 371143T^{-1}$ $(298 < T < 681.8\ K)$	this work
	${}^{\circ}G_{\alpha\text{-}CsPbI_3} = -574969.342 + 720.739961T - 158.4512T \ln T + 0.05399T^2 - 2.3333 \times 10^{-5}T^3 + 371143T^{-1}$ $(298 < T < 594\ K)$	this work
	${}^{\circ}G_{Cs_4PbI_6} = -1684327.59 + 1278.02264T - 289.8962T \ln T + 0.02123T^2 - 2.4666 \times 10^{-5}T^3 + 70771.5T^{-1}$ $(594 < T < 770\ K)$	this work
	${}^{\circ}G_{Cs_3Bi_2I_9} = -1552006.97 + 678.544824T - 211.365T \ln T - 0.142803T^2 - 0.124833 \times 10^{-5}T^3 - 300374.5T^{-1}$ $(298 < T < 872\ K)$	this work

[a]SER refers to the phase of the element stable at 298.15 K. The optimized values are marked in bold.

through χ_{CsPb/I_2} as these are defined in eq 4. In this equation, X_{CsCs/I_2} is the cation−cation pair fraction or the molar fraction of the quadruplet containing two cations Cs. For a binary system such as CsI−PbI_2, $\{X_{CsCs/I_2} + X_{CsPb/I_2} + X_{PbPb/I_2}\}$ is equal to one.

$$\chi_{CsPb/I_2} = \frac{X_{CsCs/I_2}}{X_{CsCs/I_2} + X_{CsPb/I_2} + X_{PbPb/I_2}} \quad (4)$$

The excess Gibbs energy functions used in this work are given in eq 5 for the CsI−PbI_2 system, in eq 6 for the CsI−BiI_3 system, and in eq 7 for the BiI_3−PbI_2 system. The ternary phase diagram is calculated by extrapolation from the constituting binary subsystems using the asymmetric Kohler−Toop formalism.[78] No ternary interaction parameters were used for the extrapolation of these binaries to the ternary phase diagram.

https://doi.org/10.1021/acs.jpcc.3c02696
J. Phys. Chem. C 2023, 127, 17482−17496

$$\Delta g_{CsPb/I_2} = -8000 + \chi_{CsPb/I_2}(-1500) \quad (5)$$

$$\Delta g_{CsBi/I_2} = -20200 + \chi_{CsBi/I_2}(400) + \chi_{BiCs/I_2}(-13000) \quad (6)$$

$$\Delta g_{PbBi/I_2} = -2800 + \chi_{BiPb/I_2}(-2200) \quad (7)$$

Solid Solution Description of the BiI_3–PbI_2 System. Thermodynamic modeling of the complete solid solution in the BiI_3–PbI_2 binary system and the homogeneity range in the CsI–BiI_3 binary system around $Cs_3Bi_2I_9$ is done using the compound energy formalism (CEF). Using this formalism, the assumption is that the solid is composed of sublattices with a fixed stoichiometry, with random mixing on each sublattice.[67]

The atomic scale order of the BiI_3–PbI_2 system poses the question of the proper choice of sublattices. In general, one should use the least number of optimization parameters while describing the experimental results well and resembling the physical nature. Since there is not enough experimental data available to fit the model to a brick structure, a simpler model reflecting the single-crystal XRD and EDS data from Alexander et al.[7] is selected. Their measurements indicated that Pb^{2+},Bi^{3+} and vacancies share the same site, while iodine has a fully occupied position. Therefore, the BiI_3–PbI_2 system is modeled herein as $(Pb^{2+},Bi^{3+},Va)(I^-)_2$. The Gibbs energy of this phase is expressed in eq 8; the excess Gibbs energy of the system is given in eq 9. The values used for the interaction ${}^0L$-terms in this equation are given in Table 4.

$$\begin{aligned} G - \Sigma n_i {}^\circ H_i^{SER}(298.15\ K) &= y_{Pb^{2+}} y_{I^-} \cdot {}^\circ G_{(Pb^{2+})_1(I^-)_2} + y_{Bi^{3+}} y_{I^-} \cdot {}^\circ G_{(Bi^{3+})_1(I^-)_2} + y_{Va} y_{I^-} \cdot {}^\circ G_{(Va)_1(I^-)_2} \\ &\quad + RT(y_{Pb^{2+}} \ln y_{Pb^{2+}} + y_{Bi^{3+}} \ln y_{Bi^{3+}} + y_{Va} \ln y_{Va}) + G^{excess} \end{aligned} \quad (8)$$

$$G^{excess} = {}^0L_{(Pb^{2+},Bi^{3+})_1(I^-)_2} y_{Pb^{2+}} y_{Bi^{3+}} + {}^0L_{(Pb^{2+},Va)_1(I^-)_2} y_{Pb^{2+}} y_{Va} \quad (9)$$

In eq 8, y_i is the fraction of species i in the sublattice, and ${}^\circ G_{(i)_1(j)_2}$ is the Gibbs energy of the different end-members composed of species i on the first sublattice and species j on the second sublattice. The configurational entropy term accounts for ideal mixing on the cationic sublattice.

A schematic representation of the model is given in Figure 2. In this figure, the neutral line shows at which points in this diagram the system has a net charge of zero, as this is the domain in which this model has a physical meaning. The end points of this neutral line are the end-members of this system, namely, BiI_3 and PbI_2.

The Gibbs energies of the neutrally charged end-members BiI_3 and PbI_2 can be expressed as in eqs 10 and 11, respectively. Equation 11 can be simplified to eq 12.

$${}^\circ G_{PbI_2} = {}^\circ G_{(Pb^{2+})_1(I^-)_2} \quad (10)$$

$$\frac{2}{3} {}^\circ G_{BiI_3} = \frac{2}{3} {}^\circ G_{(Bi^{3+})_1(I^-)_2} + \frac{1}{3} {}^\circ G_{(Va)_1(I^-)_2} + RT\left(\frac{1}{3}\ln\frac{1}{3} + \frac{2}{3}\ln\frac{2}{3}\right) \quad (11)$$

$${}^\circ G_{BiI_3} = {}^\circ G_{(Bi^{3+})_1(I^-)_2} + \frac{1}{2} {}^\circ G_{(Va)_1(I^-)_2} + RT\left(\ln 2 - \frac{3}{2}\ln 3\right) \quad (12)$$

The description of the three end-members of this model are given by eqs 13–15

$${}^\circ G_{(Pb^{2+})_1(I^-)_2} = {}^\circ G_{PbI_2} \quad (13)$$

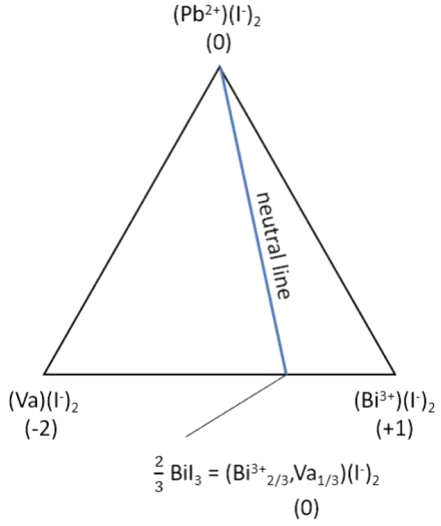

Figure 2. Graphical representation of the model for solid solution BiI_3–PbI_2 using the compound energy formalism.

$${}^\circ G_{(Bi^{3+})_1(I^-)_2} = {}^\circ G_{BiI_3} - {}^\circ G_I^{SER} - 50000 - RT\left(\ln 2 - \frac{3}{2}\ln 3\right) \quad (14)$$

$${}^\circ G_{(Va)_1(I^-)_2} = 2\,{}^\circ G_I^{SER} + 100000 \quad (15)$$

Solid Solution Description in the Ternary System. To describe the entire ternary system using the CEF, the Cs ion is also incorporated on the cationic sublattice. A vacancy is then introduced on the anionic sublattice to define the CsI end-member. The ionic species used to describe the solid solution in the ternary system are therefore $(Cs^+,Pb^{2+},Bi^{3+},Va)(I^-,Va)_2$. The corresponding Gibbs energy functions used to describe this system are given in eq 16.

$$\begin{aligned} G - \Sigma n_i {}^\circ H_i^{SER}(298.15\ K) &= y_{Cs^+} y_{I^-} \cdot {}^\circ G_{(Cs^+)_1(I^-)_2} + y_{Cs^+} y_{Va} \cdot {}^\circ G_{(Cs^+)_1(Va)_2} + y_{Pb^{2+}} y_{I^-} \cdot {}^\circ G_{(Pb^{2+})_1(I^-)_2} \\ &\quad + y_{Pb^{2+}} y_{Va} \cdot {}^\circ G_{(Pb^{2+})_1(Va)_2} + y_{Bi^{3+}} y_{I^-} \cdot {}^\circ G_{(Bi^{3+})_1(I^-)_2} \\ &\quad + y_{Bi^{3+}} y_{Va} \cdot {}^\circ G_{(Bi^{3+})_1(Va)_2} + y_{Va} y_{I^-} \cdot {}^\circ G_{(Va)_1(I^-)_2} + y_{Va} y_{Va} \cdot {}^\circ G_{(Va)_1(Va)_2} \\ &\quad + RT(y_{Cs^+} \ln y_{Cs^+} + y_{Pb^{2+}} \ln y_{Pb^{2+}} + y_{Bi^{3+}} \ln y_{Bi^{3+}} + y_{Va} \ln y_{Va}) \\ &\quad + 2RT(y_{I^-} \ln y_{I^-} + y_{Va} \ln y_{Va}) + G^{excess} \end{aligned} \quad (16)$$

with the excess Gibbs energy function, G^{excess}, as defined in eq 17. The values used for interaction parameters ${}^0L$ are given in Table 4.

$$\begin{aligned} G^{excess} &= {}^0L_{(Pb^{2+},Bi^{3+})_1(I^-)_2} y_{Pb^{2+}} y_{Bi^{3+}} + {}^0L_{(Pb^{2+},Va)_1(I^-)_2} y_{Pb^{2+}} y_{Va} \\ &\quad + {}^0L_{(Cs^+,Pb^{2+})_1(I^-)_2} y_{Cs^+} y_{Pb^{2+}} + {}^0L_{(Cs^+,Pb^{2+})_1(Va)_2} y_{Cs^+} y_{Pb^{2+}} \\ &\quad + {}^0L_{(Cs^+,Bi^{3+})_1(I^-)_2} y_{Cs^+} y_{Bi^{3+}} \end{aligned} \quad (17)$$

A graphical representation of the system is given in Figure 3.

In addition to the Gibbs energy functions given in eqs 13–15, Gibbs energy functions for the other end-members are given in eqs 18–22. The end-member consisting exclusively of vacancies, eq 22, has been destabilized using a large positive excess energy term as recommended by Sundman, Lukas and Fries.[79]

$${}^\circ G_{(Cs^+)_1(Va)_2} = {}^\circ G_{CsI} - {}^\circ G_I^{SER} - 2RT\left(\frac{1}{2}\ln\frac{1}{2} + \frac{1}{2}\ln\frac{1}{2}\right) \quad (18)$$

https://doi.org/10.1021/acs.jpcc.3c02696
J. Phys. Chem. C 2023, 127, 17482–17496

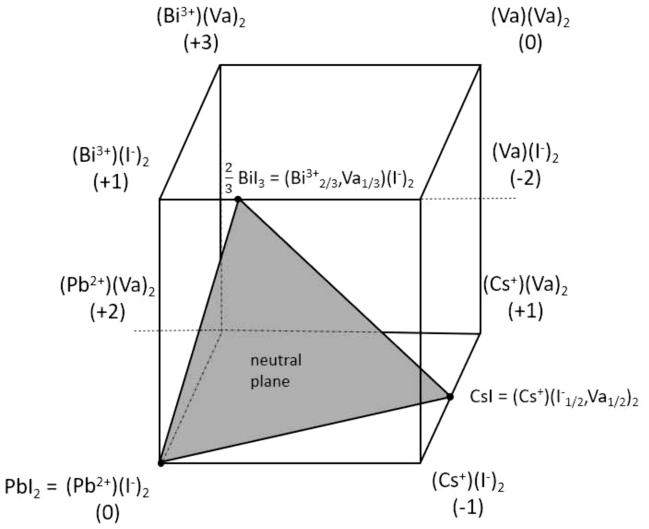

Figure 3. Graphical representation of the $(Cs^+,Pb^{2+},Bi^{3+},Va)(I^-,Va)_2$ sublattice model in the compound energy formalism. The neutral plane is the plane along which the phase diagrams of the binaries are calculated.

$$^{\circ}G_{(Cs^+)_1(I^-)_2} = {}^{\circ}G_{CsI} + {}^{\circ}G_I^{SER} - 2RT\left(\frac{1}{2}\ln\frac{1}{2} + \frac{1}{2}\ln\frac{1}{2}\right) \quad (19)$$

$$^{\circ}G_{(Pb^{2+})_1(Va)_2} = {}^{\circ}G_{PbI_2} - 2\,{}^{\circ}G_I^{SER} \quad (20)$$

$$^{\circ}G_{(Bi^{3+})_1(Va)_2} = {}^{\circ}G_{BiI_3} - 3\cdot{}^{\circ}G_I^{SER} - 50000 - RT\left(\ln 2 - \frac{3}{2}\ln 3\right) \quad (21)$$

$$^{\circ}G_{(Va)_1(Va)_2} = 100000 \quad (22)$$

Modeling the $Cs_3Bi_2I_9$ Homogeneity Range in the CEF Formalism. In the system CsI–BiI_3, the intermediate $Cs_3Bi_2I_9$ exhibits a homogeneity range spanning several mole percent. In order to model this in the CEF, an expression for this intermediate compound is used with three sublattices: $(Cs^+,Va)_3(Bi^{3+},Va)_2(I^-,Va)_9$. A graphical representation of this model is given in Figure 4.

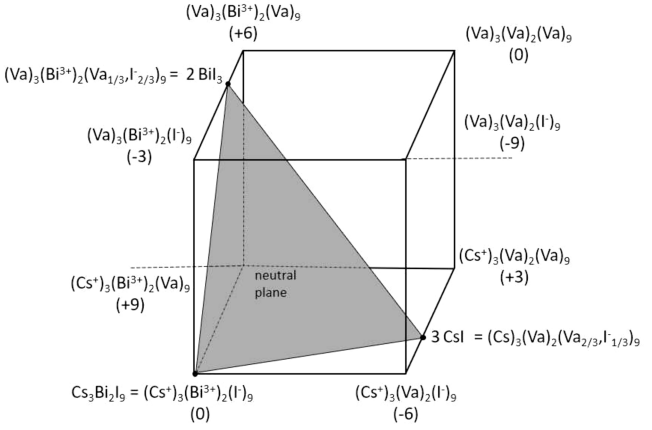

Figure 4. Graphical representation of the $(Cs^+,Va)_3(Bi^{3+},Va)_2(I^-,Va)_9$ sublattice model in the compound energy formalism. The neutral plane is the plane along which the homogeneous range around $Cs_3Bi_2I_9$ is constructed.

The Gibbs energy of the homogeneity range of $Cs_3Bi_2I_9$ is defined in eq 23, with the term G^{excess} as defined in eq 24 and the individual Gibbs energy terms for each end-member defined in eqs 25–32. The end-member consisting exclusively of vacancies, eq 32, has been destabilized using a large positive excess energy term as recommended by Sundman, Lukas, and Fries.[79] The values for the ^0L and ^1L parameters used in eq 24 are given in Table 4.

$$\begin{aligned} G - \Sigma n_i {}^{\circ}H_i^{SER}(298.15\ K) &= y_{Cs^+}y_{Bi^{3+}}y_{I^-}\cdot{}^{\circ}G_{(Cs^+)_3(Bi^{3+})_2(I^-)_9} + y_{Cs^+}y_{Bi^{3+}}y_{Va}\cdot{}^{\circ}G_{(Cs^+)_3(Bi^{3+})_2(Va)_9} \\ &+ y_{Cs^+}y_{Va}y_{I^-}\cdot{}^{\circ}G_{(Cs^+)_3(Va)_2(I^-)_9} + y_{Cs^+}y_{Va}y_{Va}\cdot{}^{\circ}G_{(Cs^+)_3(Va)_2(Va)_9} \\ &+ y_{Va}y_{Bi^{3+}}y_{I^-}\cdot{}^{\circ}G_{(Va)_3(Bi^{3+})_2(I^-)_9} + y_{Va}y_{Bi^{3+}}y_{Va}\cdot{}^{\circ}G_{(Va)_3(Bi^{3+})_2(Va)_9} \\ &+ y_{Va}y_{Va}y_{I^-}\cdot{}^{\circ}G_{(Va)_3(Va)_2(I^-)_9} + y_{Va}y_{Va}y_{Va}\cdot{}^{\circ}G_{(Va)_3(Va)_2(Va)_9} \\ &+ 3RT(y_{Cs^+}\ln y_{Cs^+} + y_{Va}\ln y_{Va}) + 2RT(y_{Bi^{3+}}\ln y_{Bi^{3+}} + y_{Va}\ln y_{Va}) \\ &+ 9RT(y_{I^-}\ln y_{I^-} + y_{Va}\ln y_{Va}) + G^{excess} \end{aligned} \quad (23)$$

$$\begin{aligned} G^{excess} &= y_{I^-}y_{Va}({}^0L_{(Cs^+)_3(Va)_2(I^-,Va)_9} + {}^1L_{(Cs^+)_3(Va)_2(I^-,Va)_9}(y_{I^-} - y_{Va})) \\ &+ y_{I^-}y_{Va}({}^0L_{(Va)_3(Bi^{3+})_2(I^-,Va)_9} + {}^1L_{(Va)_3(Bi^{3+})_2(I^-,Va)_9}(y_{I^-} - y_{Va})) \\ &+ y_{I^-}y_{Va}{}^0L_{(Cs^+,Va)_3(Bi^{3+})_2(I^-)_9} + y_{Bi^{3+}}y_{Va}{}^0L_{(Cs^+)_3(Bi^{3+},Va)_2(I^-)_9} \end{aligned} \quad (24)$$

$$^{\circ}G_{(Cs^+)_3(Bi^{3+})_2(I^-)_9} = {}^{\circ}G_{Cs_3Bi_2I_9} \quad (25)$$

$$^{\circ}G_{(Cs^+)_3(Bi^{3+})_2(Va)_9} = {}^{\circ}G_{Cs_3Bi_2I_9} - 9\,{}^{\circ}G_I^{SER} \quad (26)$$

$$^{\circ}G_{(Cs^+)_3(Va)_2(I^-)_9} = 3\,{}^{\circ}G_{CsI} + 6\,{}^{\circ}G_I^{SER} - 3RT(2\ln 2 - 3\ln 3) \quad (27)$$

$$^{\circ}G_{(Cs^+)_3(Va)_2(Va)_9} = 3\,{}^{\circ}G_{CsI} - 3\,{}^{\circ}G_I^{SER} - 3RT(2\ln 2 - 3\ln 3) \quad (28)$$

$$^{\circ}G_{(Va)_3(Bi^{3+})_2(I^-)_9} = 2\,{}^{\circ}G_{BiI_3} + 3\,{}^{\circ}G_I^{SER} - 3RT(2\ln 2 - 3\ln 3) \quad (29)$$

$$^{\circ}G_{(Va)_3(Bi^{3+})_2(Va)_9} = 2\,{}^{\circ}G_{BiI_3} - 6\,{}^{\circ}G_I^{SER} - 3RT(2\ln 2 - 3\ln 3) \quad (30)$$

$$^{\circ}G_{(Va)_3(Va)_2(I^-)_9} = 9\,{}^{\circ}G_I^{SER} + {}^{\circ}G_{(Va)_3(Va)_2(Va)_9} \quad (31)$$

$$^{\circ}G_{(Va)_3(Va)_2(Va)_9} = 100000 \quad (32)$$

RESULTS AND DISCUSSION

Characterization of Synthesized Ternary Salts. The synthesized compounds $CsPbI_3$, Cs_4PbI_6, and $Cs_3Bi_2I_9$ were found to be, respectively, yellow/green, white, and red/deep orange, in line with literature.[13,44,45] The X-ray diffraction patterns of $CsPbI_3$, Cs_4PbI_6, and $Cs_3Bi_2I_9$ are shown in Figure 5. The diffraction patterns of $CsPbI_3$ and Cs_4PbI_6 were refined by using Rietveld refinement; the pattern of $Cs_3Bi_2I_9$ was refined by using LeBail refinement. No peaks remained unidentified meaning that there are no secondary phases within detection limit. The obtained lattice parameters are listed in Table 5, along with a comparison to literature values.[32,45,80]

The calculated densities are also listed in Table 5. The density of the salts as compared to liquid Pb or LBE is of practical importance. The density of Pb and LBE at various temperatures is given in the Handbook;[81] until 1100 K, it stays above 10 $g\cdot cm^{-3}$. Based on the density at room temperature, this means that if these ternary compounds are formed in the coolant vessel, they will float on top of the coolant.

https://doi.org/10.1021/acs.jpcc.3c02696
J. Phys. Chem. C 2023, 127, 17482–17496

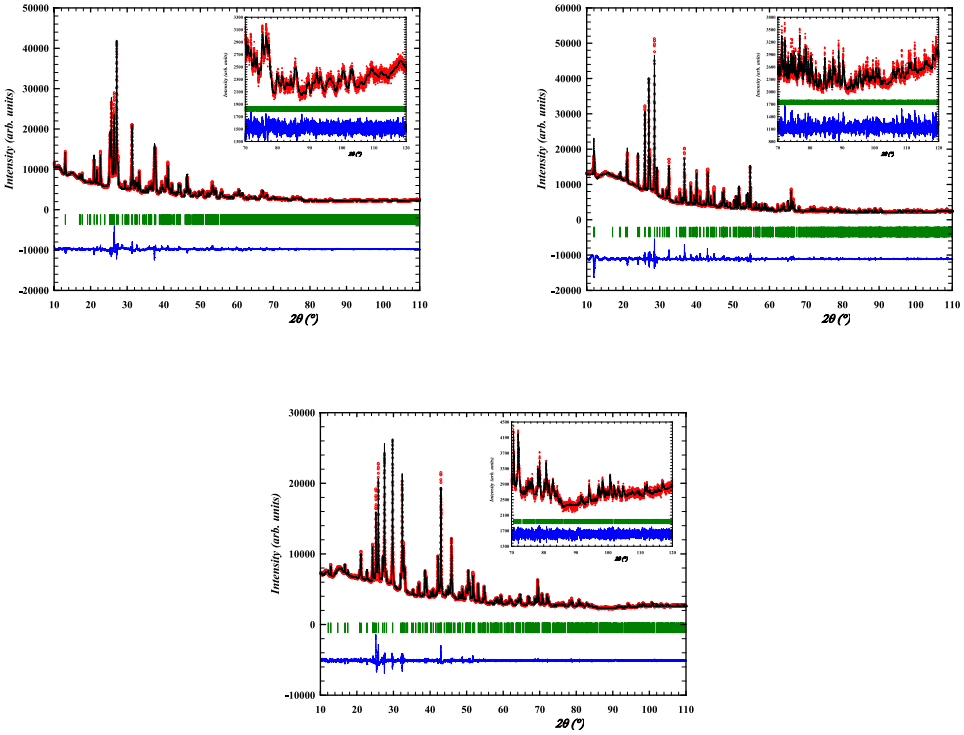

Figure 5. Experimental (Y_{obs}, in red) and calculated (Y_{calc}, in black) XRD patterns of $CsPbI_3$ (top right), Cs_4PbI_6 (top left), and $Cs_3Bi_2I_9$ (bottom) at ambient conditions. The difference between calculated and experimental intensities, $Y_{obs} - Y_{calc}$ is shown in blue. The angular positions of Bragg reflections are shown in green. Measurement is λ = Cu K_α.

Table 5. Crystallographic Information for Synthesised $CsPbI_3$, Cs_4PbI_6, and $Cs_3Bi_2I_9$, As Used and Obtained in This Work, Compared with Literature Values.[32,45,80a]

compound	#	a (Å)	b (Å)	c (Å)	γ (°)	volume (Å^3)	ρ (g·cm^{-3})	source
$CsPbI_3$	62	10.455(2)	4.8015(6)	17.773(2)	90	892.2(2)	5.366(1)	this work
	62	10.4581(3)	4.8017(1)	17.7761(5)	120	892.66	5.36	[80]
Cs_4PbI_6	167	14.5578(7)	14.5578(7)	18.300(1)	120	3348.7(3)	4.4500(4)	this work
	167	14.528	14.528	18.313	120	3347.35	4.47	[45]
$Cs_3Bi_2I_9$	194	8.4134(4)	8.4134(4)	21.196(1)	120	1299.4(1)	5.0066(4)	this work
	194	8.4116	8.4116	21.182	120	1297.94	5.01	[32]

[a]# = number of crystallographic space group. Densities calculated based on crystal structure. Standard uncertainties given by FullProf are multiplied by 10.

DSC of the End Members and Compounds. The DSC results of the purchased compounds CsI, PbI_2, and BiI_3 were compared to the literature values. The measured melting points for CsI (904 ± 5 K), PbI_2 (687 ± 5 K), and BiI_3 (665 ± 5 K) are compared with literature values in Table 6. The melting point for CsI was found to agree very well, while those for PbI_2 and BiI_3 are, respectively, a bit higher and lower than found in literature. The compounds CsI and BiI_3 do not have polymorphs. PbI_2 has a CdI_2-like structure and exhibits polytypism. However, polytype 2H is by far the most present and the polytypic transition does not come with a large enthalpy change.[71] Therefore, the polytypism of PbI_2 is further neglected in this work. The phase transition and melting point of $CsPbI_3$ were found to agree well with literature. For the peritectically decomposing compound Cs_4PbI_6, the heat effect on the first cycle of the synthesized compound was taken and found to be some 20 K higher than the values reported in literature.[42,43] The melting temperature of freshly synthesized $Cs_3Bi_2I_9$ on the first DSC cycle was found to be (870 ± 5) K, which drops by approximately 10° upon subsequent cycles and a small prepeak appearing. This might be attributed to the homogeneity range as described by Kun et al.;[30] in this work, the temperature on the first heating ramp was taken as the melting point of $Cs_3Bi_2I_9$. Values as determined in this work and in the literature for all six compounds are collected in Table 6, alongside known melting enthalpies (e.g., CsI, PbI_2 and BiI_3). There are, to the best of our knowledge, no experimental data available on the melting enthalpy of intermediates $CsPbI_3$ and Cs_4PbI_6. There is, however, data on the melting enthalpy of $Cs_3Bi_2I_9$, reported by Kun et al.[30]

Binary Phase Diagram Studies: Calorimetric Measurements and Modeling. *Binary System CsI–BiI_3.* The experimentally measured thermal transitions in the CsI–BiI_3 system with their interpretation are given in Table S.2. As shown in Figure 6, the DSC results can be interpreted in line with the previously reported phase diagrams of Plyuschev et al. and Kun et al.[28,30] This interpretation is further underpinned by post-DSC analysis (see Table S.1), in which only binary mixtures of $Cs_3Bi_2I_9$ with one of the end-members CsI or BiI_3 were found. However, for the measurements at $0.1 \leq x(BiI_3) \leq 0.4$, extra thermal arrests were also detected at around 724 K. A series of quenching and synthesis experiments with phase

https://doi.org/10.1021/acs.jpcc.3c02696
J. Phys. Chem. C 2023, 127, 17482−17496

Table 6. Phase Transition Temperatures and Melting Enthalpies of the Compounds As Measured in This Research Compared to Literature[a]

species	T (K)	transition type	$\Delta_{tr}H^{\circ}_{m}(T_{tr})$ (kJ·mol^{-1})	ref
CsI	904 ± 5	congr. melting		this work, exp.
	905		25.7	this work, mod.
	914			43
	903.8 ± 0.2		24.0 ± 0.2	82
	905 ± 2		25.65 ± 0.4	83
	902.4 ± 5			69
PbI_2	580	polytypism	0.339	71
	687 ± 5	congr. melting		this work, exp.
	682.9		23.5	this work, mod.
	677			43
	679		23.344	71
BiI_3	665 ± 5	congr. melting		this work, exp.
	681.8		39.1	this work, mod.
	681.7		39.1 ± 0.3	74
$CsPbI_3$	599 ± 5	polymorphism		this work, exp.
	594		14.2	this work, mod.
	600			43
	594.8−599		14.2 ± 0.5	50
	595			84
	593		14.1 ± 0.24	46
	758 ± 5	congr. melting		this work, exp.
	770		26.78	this work, mod.
	754			42
	749			43
	757			84
Cs_4PbI_6	759 ± 5	peritectic		this work, exp.
	769		71.31	this work, mod.
	737			42
	741			43
$Cs_3Bi_2I_9$	870 ± 5	congr. melting		this work, exp.
	872		177	this work, mod.
	907			28
	905 ± 5		148 ± 2.2	30

[a]The values referred to as "this work" are the experimentally determined (exp.) values and the values used in the modeling (mod.).

analysis (see Table S.1) did not show the presence of any other compound besides $Cs_3Bi_2I_9$ and CsI. The trend in composition versus heat (see Figure S.3) indicates that the effect cannot be ascribed to polymorphism in $Cs_3Bi_2I_9$ nor to a compound at $x(BiI_3) = 0.25$, a composition that is known for other cesium bismuth halide phases. A high-temperature polymorph was not found upon a quenching experiment (Table S.1). A further possible explanation would be the existence of a high-temperature phase at $x(BiI_3) = 0.2$, corresponding to the maximum in the heat release of the DSC curves in the composition range, but quenching experiments did not reveal

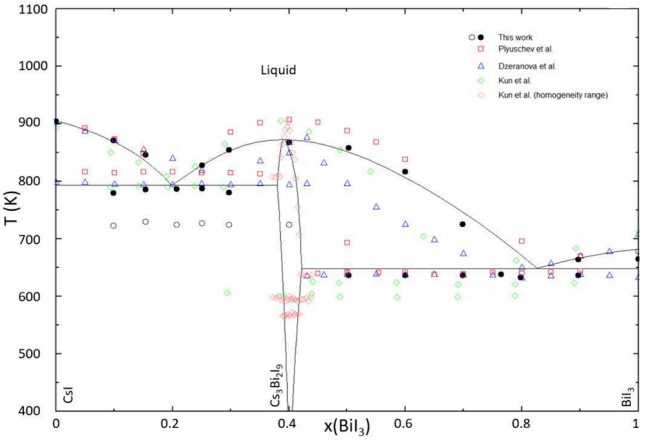

Figure 6. Phase diagram of the CsI−BiI_3 binary system, as calculated with the thermodynamic model presented in Table 4. The experimental data shown on the phase diagram is from Plyuschev et al.[28] (green squares), Dzeranova et al.[29] (blue triangles), Kun et al.[30] (red and orange squares), and this work (black circles).

the existence of such a phase either (Table S9). In absence of additional evidence on the existence of such a high-temperature phase, this thermal effect was not accounted for in the model.

The calculated phase diagram of the CsI−BiI_3 system is shown in Figure 6. The calculated invariant equilibria are given in Table 7. The CALPHAD model agrees well with the data measured in this work. The mixing enthalpy of this system is shown in Figure S.2 at T = 1000 K. The CsI−BiI_3 system is characterized by two eutectic points, formed between $Cs_3Bi_2I_9$ and, respectively, CsI and BiI_3. The eutectic compositions between $Cs_3Bi_2I_9$ and CsI is well-defined. In the current work, the composition was found to be $x(BiI_3) = 0.22 \pm 0.005$, matching with refs 28 and 30. The eutectic composition reported by ref 29 differs, but their figure is judged to be unreliable on the composition axis. The eutectic temperature corresponding to this event varies between T = (784 ± 10) K (this work) and T = 795 K[29]. The eutectic composition between $Cs_3Bi_2I_9$ and BiI_3 is ill-defined, varying between $x(BiI_3) = 0.70$[28] and $x(BiI_3) = 0.86$[30]. Our experimental ($x(BiI_3) = 0.77$) as well as optimized ($x(BiI_3) = 0.80$) values are intermediate in the range of reported values. The temperature of the eutectic as reported in literature is slightly higher than modeled and measured in this work. The measured congruent melting temperature of intermediate $Cs_3Bi_2I_9$ is not entirely in agreement with the data from the aforementioned literature. There is, however, good agreement between the model and the available experimental data for compositions $x(BiI_3) \leq 0.8$. The homogeneity range of $Cs_3Bi_2I_9$, as measured by Kun et al.,[30] has been included in the model. The model fits well with the available experimental data at temperatures of T = 630 K and above; the homogeneity range is not quite as wide at lower temperatures, as measured by Kun et al. at 600 and 570 K. The value of the melting enthalpy of the non-stoichiometric compound $Cs_3Bi_2I_9$, as predicted using the CALPHAD model presented in this work, is slightly higher. The congruent melting point of this compound, however, is predicted to be at $x(BiI_3) = 0.39$, rather than $x(BiI_3) = 0.40$, like its stoichiometry suggests at face value. Further investigation into the exact temperature and composition of this congruent melting point is necessary to assess the accuracy

https://doi.org/10.1021/acs.jpcc.3c02696
J. Phys. Chem. C 2023, 127, 17482−17496

of the predicted melting enthalpy. Overall, the current model captures the system well within the sometimes rather widespread of experimental results.

Table 7. Invariant Points Are on the CsI−BiI_3 Phase Diagram[a]

reaction	type	$x(BiI_3)$	T (K)	ref
$Cs_3Bi_2I_9$ + CsI = L	eutectic	0.22	784	this work, exp.
		0.21	790	this work, mod.
		0.22	814	28
		0.30	795	29
		0.22	790	30
$Cs_3Bi_2I_9$ = L	congr. melting	0.40	870	this work, exp
		0.39	872	this work, mod.
		0.40	907	28
		0.40	905	30
$Cs_3Bi_2I_9$ + BiI_3 = L	eutectic	0.77	636	this work, exp
		0.80	640	this work, mod.
		0.86	638	28
		0.75	637	29
		0.70	625	30

[a]The uncertainties on the experimental results of this work on composition are estimated to be ±0.005; the uncertainties on temperature for mixtures are estimated to be ±10 K.

Binary System CsI−PbI_2. The experimentally measured thermal transitions with their interpretation are given in Table S.4. The current results agree well with the liquidus line of Ilyasov et al.[42] and the phase diagram of Belyaev et al.[43] The peritectic decomposition temperature of Cs_4PbI_6 varies a bit. The mixing enthalpy of this system is shown in Figure S.2 at T = 1000 K. Post-DSC XRD studies at $x(PbI_2)$ = 0.20 indicated the presence of three compounds, viz. Cs_4PbI_6, $CsPbI_3$ and CsI. Based on the presence of only these three compounds, we can conclude that the compounds on the Cs-richer and Cs-poorer sides are, respectively, CsI and $CsPbI_3$. Moreover, the difficulty in obtaining a pure Cs_4PbI_6 single crystal is consistent with the presence of a peritectic decomposition near a eutectic equilibrium. The XRD pattern of the sample with a mixture at $x(PbI_2)$ = 0.50 showed the presence of just one compound: δ-$CsPbI_3$. The XRD pattern of the sample with a mixture at $x(PbI_2)$ = 0.70 was analyzed using HighScore[85] analysis; only $CsPbI_3$ and PbI_2 were found. From these crystallographic analyses the number of compounds in the pseudobinary phase diagram CsI−PbI_2 was found to be limited to two: Cs_4PbI_6 and $CsPbI_3$. The post-DSC XRD studies are summarized in Table S.1.

The calculated phase diagram of this system is presented in Figure 7. The calculated invariant equilibria are given in Table 8, along with the corresponding experimental data. Calculations performed with the CALPHAD model displayed in Figure 7 show good agreement with the measured invariant points obtained in this work. The overall agreement with the data reported in the literature is also good, though there is a slight discrepancy between the calculated liquidus at $x(PbI_2)$ = 0.5 and 0.79 and the experimental data by Ilyasov et al.[42] and Belyaev et al.[43]

Binary System BiI_3−PbI_2. The experimentally measured temperatures with their interpretation are given in Table S.3. Upon first inspection, several of the peaks were quite broad. This could indicate that solidus and liquidus equilibria overlap upon measurement. Thus, the data were interpreted by taking

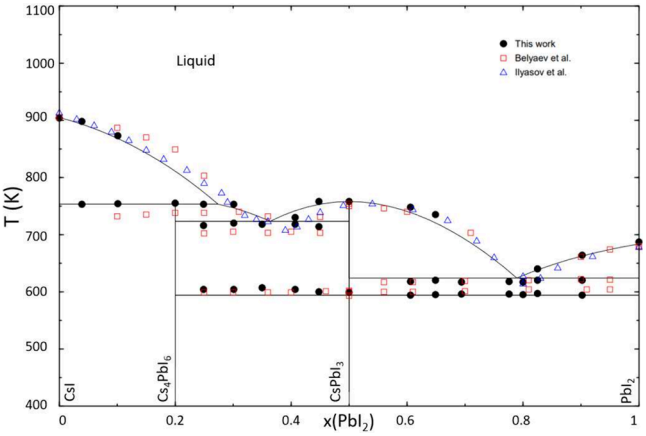

Figure 7. Phase diagram of the CsI−PbI_2 binary system as calculated with the thermodynamic model presented in the main text. The experimental data shown on the phase diagram is from Ilyasov et al.[42] (blue squares), Belyaev et al.[43] (red squares), and this work (black circles).

Table 8. Invariant Points on the Pseudo-Binary Section CsI−PbI_2[a]

reaction	type	$x(PbI_2)$	T (K)	ref
Cs_4PbI_6 = CsI + L	peritectic	0.20	754	this work, exp.
		0.20	758	this work, mod.
		0.20	737	42
		0.20	741	43
Cs_4PbI_6 + $CsPbI_3$ = L	eutectic	0.38	718	this work, exp.
		0.36	722	this work, mod.
		0.39	707	42
		0.40	705	43
δ-$CsPbI_3$ = α-$CsPbI_3$	polymorphism	0.50	599	this work, exp.
		0.50	594	this work, mod.
		0.50	600	43
		0.50	595	50
		0.50	595	84
		0.50	593	46
α-$CsPbI_3$ = L	congr. melting	0.50	758	this work, exp.
		0.50	770	this work, mod.
		0.50	754	42
		0.50	749	43
		0.50	757	84
PbI_2 + $CsPbI_3$ = L	eutectic	0.80	618	this work, exp.
		0.78	621	this work, mod.
		0.80	614	42
		0.80	615	43

[a]The uncertainties on the experimental results of this work on composition are estimated to be ±0.005; the uncertainties on temperature for mixtures are estimated to be ±10 K.

the onset temperature of every peak on heating as the *solidus* line and the maximum as the *liquidus* line. In this way, the trend of the measured points indicates the formation of a complete solid solution over the whole composition range. Given the similarities in the crystal structures of PbI_2 and BiI_3, a structure where the positions of Pb^{2+} are occupied by Bi^{3+} and holes can be hypothesized, like was done by Dmitriev et al.[55] and Alexander et al.[6,7] Alexander[7] also reports the only DSC measurement on a mixture in this system that is known to us; that single point is in line with the current results. The

https://doi.org/10.1021/acs.jpcc.3c02696
J. Phys. Chem. C 2023, 127, 17482−17496

mixing enthalpy of this system is shown in Figure S.2 at T = 1000 K. The post-DSC XRD studies of the BiI_3–PbI_2 axis, as summarized in Table S.1, indicated the presence of crystalline material, the structure of which we could not resolve. The X-ray diffraction patterns are shown in Figure S.1. Recently, Alexander et al.[6,7] reported an XRD pattern of a sample at $x(PbI_2)$ = 0.50 and the results were ascribed to a layered structure that is disordered. TEM analysis indicated Pb-rich and Bi-rich "bricks" at the nanoscale.

The calculated phase diagram of this system is presented in Figure 8. It shows good agreement between the measured data

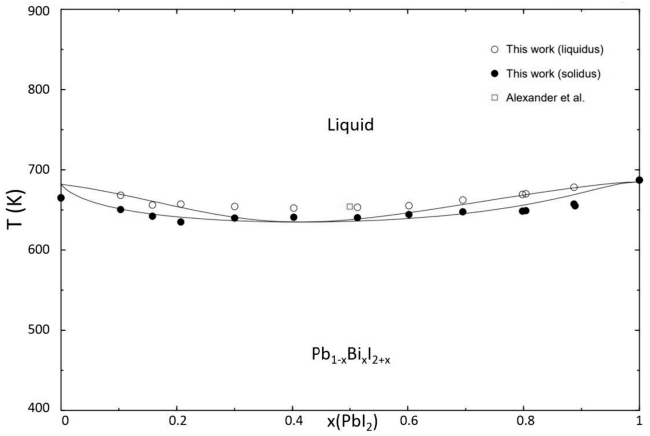

Figure 8. Phase diagram of the BiI_3–PbI_2 binary system as calculated with the thermodynamic model presented in Table 4. The peak onset temperature was used to determine the solidus data (black solid circles), and the temperature at the peak maximum was used to determine the liquidus data (black open circles).

and the thermodynamic model. The entire composition range between PbI_2 and BiI_3 consists of a solid solution with composition $Pb_{1-x}Bi_xI_{2+x}$. The only available literature data point of Alexander[7] fits with the current experimentally measured and modeled results. The solidus and liquidus lines cross at $x(PbI_2)$ = 0.41 and T = 634 K. The atomic scale structure of BiI_3–PbI_2 mixtures, which we consider here to be a solid solution, deserves dedicated analysis. Both structures are layered, so the solid solution will be a mixture of Pb, Bi and vacancies. The question is whether this mixing is completely random, or if there is a strong preference of the vacancies and Bi to be together.

Ternary Phase Diagram Studies: Modeling and Experiments. The ternary phase diagram CsI–PbI_2–BiI_3 was calculated using only the binary interaction parameters, as described *supra*. The liquidus projection of the ternary phase diagram is shown in Figure 9. An isotherm at T = 300 K is given in Figure 10, showing the stable phases at room temperature. The ternary eutectic points and the phase equilibria in the pseudobinary section $Cs_3Bi_2I_9$–$CsPbI_3$ are discussed *infra*. Moreover, some miscellaneous points are described.

Ternary Eutectic Equilibria. The calculated ternary phase field reveals three ternary eutectic points. The calculated compositions are given alongside the experimentally measured phase transition temperatures in Table 9. As can be concluded from the Table, the eutectic temperatures are accurately reproduced by the model. It is observed that the ternary eutectic points are all located close to the CsI–PbI_2 side.

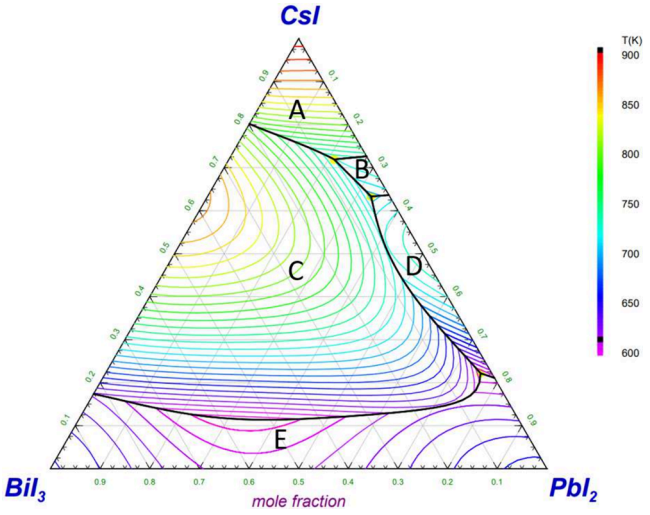

Figure 9. Liquidus surface of the CsI–PbI_2–BiI_3 ternary system as calculated with the thermodynamic model presented in Table 4. The precipitate target phases labeled A–E are as follows: CsI (A), Cs_4PbI_6 (B), $Cs_3Bi_2I_9$ (C), $CsPbI_3$ (D), and $Pb_{1-x}Bi_xI_{2+x}$ (E).

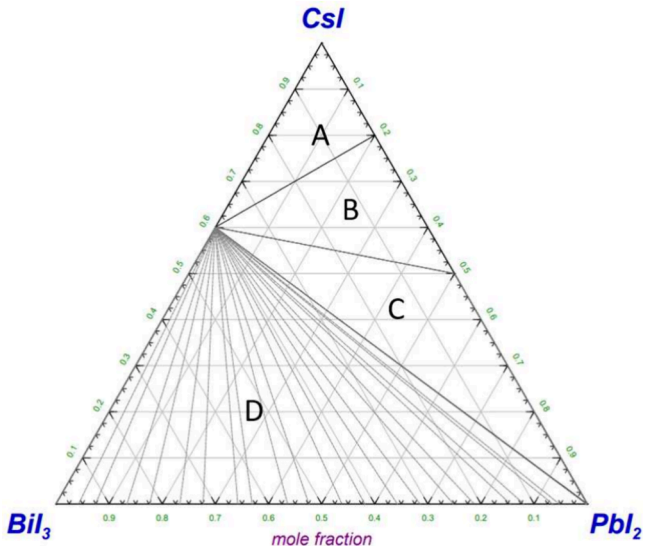

Figure 10. Isothermal section of the CsI–PbI_2–BiI_3 ternary system at T = 300 K as calculated with the thermodynamic model presented in Table 4. The phases on the diagram labeled A–D are as follows: CsI + $Cs_3Bi_2I_9$ + Cs_4PbI_6 (A), $Cs_3Bi_2I_9$ + $CsPbI_3$ + Cs_4PbI_6 (B), $Cs_3Bi_2I_9$ + $CsPbI_3$ + PbI_2 (C), $Pb_{1-x}Bi_xI_{2+x}$ + $Cs_3Bi_2I_9$ (D).

Pseudobinary Section $Cs_3Bi_2I_9$–$CsPbI_3$. The measured phase transition temperatures as obtained by DSC are given together with their interpretation in Table S.5 and drawn on top of the modeled phased diagram in Figure 11. The experimentally measured liquidus curve and eutectic events agree well with the points predicted by the thermodynamic model. The experimental data point at $x(CsPbI_3)$ = 0.7 and T = 680 K is possibly a measurement error, as it seems to be an outlier compared to similar compositions. The eutectic point on this pseudobinary section is at $x(CsPbI_3)$ = 0.91 and T = 740 K. No indication for the existence of quaternary compounds was found.

Ternary System: Miscellaneous Points. Based on the reports by Hu et al.,[10] a sharp decrease of the transition temperature δ-$CsPbI_3$ = α-$CsPbI_3$ was expected when small

https://doi.org/10.1021/acs.jpcc.3c02696
J. Phys. Chem. C 2023, 127, 17482–17496

Table 9. Calculated Ternary Eutectic Compositions with Phase Transitions Experimentally Found at Those Compositions[a]

x(CsI)	x(PbI_2)	x(BiI_3)	T_c (K)	T_e (K)	equilibrium	equilibrium reaction
0.72	0.21	0.07	739	729	eutectic	$CsI + Cs_3Bi_2I_9 + Cs_4PbI_6 = L$
0.63	0.33	0.04	715	707	eutectic	$Cs_3Bi_2I_9 + Cs_4PbI_6 + CsPbI_3 = L$
0.22	0.76	0.02	621	617	eutectic	$Cs_3Bi_2I_9 + CsPbI_3 + Pb_{1-x}Bi_xI_{2+x} = L$

[a]T_c = calculated temperature; T_e = experimentally measured temperature. The uncertainties on the measured temperatures are estimated to be ±10 K.

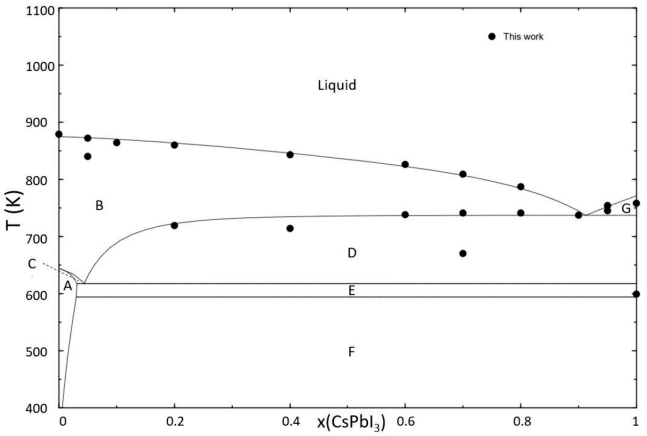

Figure 11. Phase diagram of the $Cs_3Bi_2I_9$–$CsPbI_3$ pseudobinary system as calculated with the thermodynamic model presented in Table 4. The experimental data shown in the phase diagram were obtained in this work. The phases on the diagram labeled A-G are as follows: $Cs_3Bi_2I_9 + Pb_{1-x}Bi_xI_{2+x}$ (A), $Cs_3Bi_2I_9 + L'$ (B), $Cs_3Bi_2I_9 + Pb_{1-x}Bi_xI_{2+x} + L'$ (C), α-$CsPbI_3 + Cs_3Bi_2I_9 + L'$ (D), α-$CsPbI_3 + Cs_3Bi_2I_9 + Pb_{1-x}Bi_xI_{2+x}$ (E), δ-$CsPbI_3 + Cs_3Bi_2I_9 + Pb_{1-x}Bi_xI_{2+x}$ (F), α-$CsPbI_3 + L'$ (G).

amounts of BiI_3 were added. However, three attempts on this axis with compositions x($CsPbI_3$) = 0.96 and x = 0.98 did not result in a sharp drop of the temperature. The found temperature values for the δ-$CsPbI_3 \rightarrow \alpha$-$CsPbI_3$ transition are, respectively, 586 and 589 K, which is just a few degrees below the reported values for the phase transitions as given in Table 6, but definitely not stabilizing the perovskite phase down to room temperature. The obtained results are consistent with the conclusion of Zhang et al.[57,58] who found computationally that stabilization of the perovskite phase cannot be ascribed to the physical properties of Bi^{3+}. However, the current results also do not support the destabilizing effect, as suggested in ref 57. For thin films, it was also found that α-$CsPbI_3$ is not stabilized by the incorporation of Bi-ions.[59]

Other compositions in the ternary field that have been investigated with DSC are reported in Table 10, along with the temperatures calculated with the CALPHAD model. The measured points show a slight deviation from the calculated values but are close enough that further optimization of the ternary field was deemed unnecessary.

CONCLUSIONS

To study the liquidus surface of the ternary system CsI–PbI_2–BiI_3, the constituting binary salt systems were investigated for the first time (BiI_3–PbI_2) or subjected to renewed investigation (CsI–PbI_2 and CsI–BiI_3). Based on our DSC results, the BiI_3–PbI_2 system seems to form a continuous solid solution over the whole composition range. In general, the CsI–PbI_2 and CsI–BiI_3 systems behave as reported previously in literature. The three binary systems were modeled and extrapolated to the ternary phase field. The predicted ternary eutectic points and section $Cs_3Bi_2I_9$–$CsPbI_3$ were experimentally measured. They agree well with the predictions by the CALPHAD model.

Using the obtained liquidus surface, the state (solid or liquid) of any mixture of CsI–PbI_2–BiI_3 can easily be determined at any given temperature and composition. Depending on the temperature of interest, this model predicts which phases will be thermodynamically stable.

Two limitations of our current study for the safety assessment of the LFRs and LBE-cooled reactors are given by the fact that we studied only the ternary salt field, mainly focusing on the determination of the liquidus surface. Since most of the Pb and Bi will be present as liquid metals, thermodynamic studies into the Pb–Bi–Cs–I system are also necessary. Moreover, under high operating temperatures or severe accident conditions, the gas phase properties might

Table 10. Measured and Calculated Invariant Equilibria in Ternary Phase Field CsI–PbI_2–BiI_3[a]

x(CsI)	x(PbI_2)	x(BiI_3)	T_c (K)	T_e (K)	equilibrium	equilibrium reaction
0.36	0.36	0.28	772	752	liquidus	$Cs_3Bi_2I_9 + L'' = L$
			649	621		$Cs_3Bi_2I_9 + CsPb_{1-x}Bi_xI_{3+x} + L' = Cs_3Bi_2I_9 + L''$
			618	608		δ-$CsPbI_3 + Cs_3Bi_2I_9 + CsPb_{1-x}Bi_xI_{3+x} = Cs_3Bi_2I_9 + CsPb_{1-x}Bi_xI_{3+x} + L'$
0.57	0.37	0.06	736	751	liquidus	α-$CsPbI_3 + Cs_3Bi_2I_9 + L' = L$
			708	686	eutectic	α-$CsPbI_3 + Cs_4PbI_6 + Cs_3Bi_2I_9 = \alpha$-$CsPbI_3 + Cs_3Bi_2I_9 + L'$
				667		
				608		
			594	584	polymorphism	δ-$CsPbI_3 + Cs_4PbI_6 + Cs_3Bi_2I_9 = \alpha$-$CsPbI_3 + Cs_4PbI_6 + Cs_3Bi_2I_9$
0.50	0.48	0.02	758	759	liquidus	α-$CsPbI_3 = L$
			594	587	polymorphism	δ-$CsPbI_3 + Cs_3Bi_2I_9 + CsPb_{1-x}Bi_xI_{3+x} = \alpha$-$CsPbI_3 + Cs_3Bi_2I_9 + CsPb_{1-x}Bi_xI_{3+x}$
0.50	0.49	0.01	756	762	liquidus	α-$CsPbI_3 = L$
			594	584	polymorphism	δ-$CsPbI_3 + Cs_3Bi_2I_9 + CsPb_{1-x}Bi_xI_{3+x} = \alpha$-$CsPbI_3 + Cs_3Bi_2I_9 + CsPb_{1-x}Bi_xI_{3+x}$

[a]T_c = calculated temperature; T_e = experimentally measured temperature. The uncertainties on the measured temperatures are estimated to be ±10 K.

https://doi.org/10.1021/acs.jpcc.3c02696
J. Phys. Chem. C 2023, 127, 17482–17496

become important too. The temperature window of applicability of the current model can however be bound to the maximum temperature in the coolant vessel.

■ ASSOCIATED CONTENT

Supporting Information

The Supporting Information is available free of charge at https://pubs.acs.org/doi/10.1021/acs.jpcc.3c02696.

Tables S.1−S.5 and Figures S.1−S.3 (PDF)

■ AUTHOR INFORMATION

Corresponding Author

Anna L. Smith − *Reactor Physics and Nuclear Materials, Radiation Science and Technology Department, Faculty of Applied Sciences, Delft University of Technology, Delft 2629JB, The Netherlands;* orcid.org/0000-0002-0355-5859; Email: a.l.smith@tudelft.nl

Authors

Andries van Hattem − *Reactor Physics and Nuclear Materials, Radiation Science and Technology Department, Faculty of Applied Sciences, Delft University of Technology, Delft 2629JB, The Netherlands;* orcid.org/0000-0001-8814-4049

Dennis Alders − *Reactor Physics and Nuclear Materials, Radiation Science and Technology Department, Faculty of Applied Sciences, Delft University of Technology, Delft 2629JB, The Netherlands;* orcid.org/0009-0004-2206-8329

Rudy J. M. Konings − *Reactor Physics and Nuclear Materials, Radiation Science and Technology Department, Faculty of Applied Sciences, Delft University of Technology, Delft 2629JB, The Netherlands*

Complete contact information is available at: https://pubs.acs.org/10.1021/acs.jpcc.3c02696

Notes

The authors declare no competing financial interest.

■ ACKNOWLEDGMENTS

This work has received funding from the Euratom research and training programme 2019−2020 through the Research Project PASCAL (Proof of Augmented Safety Conditions in Advanced Liquid-metal-cooled systems) under Grant Agreement No. 945341.

■ REFERENCES

(1) Xu, Q.; Li, C.; Nie, J.; Guo, Y.; Wang, X.; Zhang, B.; Ouyang, X. Highly Sensitive and Stable X-ray Detector Based on a 0D Structural Cs_4PbI_6 Single Crystal. *J. Phys. Chem. Lett.* **2021**, *12*, 287−293.

(2) Li, Y.; Chen, L.; Gao, R.; Liu, B.; Zheng, W.; Zhu, Y.; Ruan, J.; Ouyang, X.; Xu, Q. Nanosecond and Highly Sensitive Scintillator Based on All-Inorganic Perovskite Single Crystals. *ACS Appl. Mater. Interfaces* **2022**, *14*, 1489−1495.

(3) Li, Y.; Chen, L.; Ouyang, X.; Zhao, K.; Xu, Q. Cryogenic Scintillation Performance of Cs_4PbI_6 Perovskite Single Crystals. *Inorg. Chem.* **2022**, *61*, 7553−7559.

(4) Zhang, J.; Li, A.; Li, B.; Yang, M.; Hao, X.; Wu, L.; Zhao, D.; Xia, G.; Ren, Z.; Tian, W.; et al. Top-Seed Solution-Based Growth of Perovskite $Cs_3Bi_2I_9$ Single Crystal for High Performance X-ray Detection. *ACS Photonics* **2022**, *9*, 641−651.

(5) Ge, S.; Wang, Y.; Xiang, Z.; Cui, Y. Reset Voltage-Dependent Multilevel Resistive Switching Behavior in $CsPb_{1-x}Bi_xI_3$ Perovskite-Based Memory Device. *ACS Appl. Mater. Interfaces* **2018**, *10*, 24620−24626.

(6) Alexander, G. C.; Krantz, P. W.; Jung, H. J.; Davis, S. K.; Xu, Y.; Dravid, V. P.; Chandrasekhar, V.; Kanatzidis, M. G. Controllable Nonclassical Conductance Switching in Nanoscale Phase-Separated $(PbI_2)_{1-x}(BiI_3)_x$ Layered Crystals. *Adv. Mater.* **2021**, *33*, 2103098.

(7) Alexander, G. Exploratory synthesis and characterization of heavy metal halide semiconductors: unveiling new properties and structures. *Ph.D. Thesis*, Northwestern University, 2020.

(8) Wang, Y.-K.; Yuan, F.; Dong, Y.; Li, J.-Y.; Johnston, A.; Chen, B.; Saidaminov, M. I.; Zhou, C.; Zheng, X.; Hou, Y.; et al. All-Inorganic Quantum-Dot LEDs Based on a Phase-Stabilized α-$CsPbI_3$ Perovskite. *Angew. Chem., Int. Ed.* **2021**, *60*, 16164−16170.

(9) Fakharuddin, A.; Gangishetty, M. K.; Abdi-Jalebi, M.; Chin, S.-H.; bin Mohd Yusoff, A. R.; Congreve, D. N.; Tress, W.; Deschler, F.; Vasilopoulou, M.; Bolink, H. J. Perovskite light-emitting diodes. *Nature Electronics* **2022**, *5*, 203−216.

(10) Hu, Y.; Bai, F.; Liu, X.; Ji, Q.; Miao, X.; Qiu, T.; Zhang, S. Bismuth incorporation stabilized α-$CsPbI_3$ for fully inorganic perovskite solar cells. *ACS Energy Letters* **2017**, *2*, 2219−2227.

(11) Hutter, E. M.; Savenije, T. J. Thermally activated second-order recombination hints toward indirect recombination in fully inorganic $CsPbI_3$ perovskites. *ACS Energy Letters* **2018**, *3*, 2068−2069.

(12) Johansson, M. B.; Zhu, H.; Johansson, E. M. Extended photoconversion spectrum in low-toxic bismuth halide perovskite solar cells. *J. Phys. Chem. Lett.* **2016**, *7*, 3467−3471.

(13) Johansson, M. B.; Philippe, B.; Banerjee, A.; Phuyal, D.; Mukherjee, S.; Chakraborty, S.; Cameau, M.; Zhu, H.; Ahuja, R.; Boschloo, G.; et al. Cesium bismuth iodide solar cells from systematic molar ratio variation of CsI and BiI_3. *Inorg. Chem.* **2019**, *58*, 12040−12052.

(14) Wang, Y.; Guan, X.; Li, D.; Cheng, H.-C.; Duan, X.; Lin, Z.; Duan, X. Chemical vapor deposition growth of single-crystalline cesium lead halide microplatelets and heterostructures for optoelectronic applications. *Nano Research* **2017**, *10*, 1223−1233.

(15) Bonomi, S.; Malavasi, L. Physical and chemical vapor deposition methods applied to all-inorganic metal halide perovskites. *Journal of Vacuum Science & Technology A: Vacuum, Surfaces, and Films* **2020**, *38*, 060803.

(16) U.S. DOE Nuclear Energy Research Advisory Committee; Generation IV International Forum, A Technology Roadmap for Generation IV Nuclear Energy Systems. 2002; https://www.gen-4.org/gif/jcms/c_40481/technology-roadmap, Date of last access: June 9, 2023.

(17) Weeks, J. Lead, bismuth, tin, and their alloys as nuclear coolants. *Nucl. Eng. Des.* **1971**, *15*, 363−372.

(18) Zhang, J. Lead−Bismuth Eutectic (LBE): A Coolant Candidate for Gen. IV Advanced Nuclear Reactor Concepts. *Adv. Eng. Mater.* **2014**, *16*, 349−356.

(19) Zverev, D.; Neevin, S.; Doronkov, D.; Sokolova, L. Nuclear Ship Reactor Installations: From Gen 1 to 5. *Atomic Energy* **2020**, *129*, 1−7.

(20) Troyanov, V. M.; Toshinsky, G. I.; Stepanov, V. S.; Petrochenko, V. V. Lead-bismuth cooled reactors: history and the potential of development. Part 1. History of development. *Nuclear Energy and Technology* **2022**, *8*, 187−195.

(21) Abderrahim, H. A.; Kupschus, P.; Malambu, E.; Benoit, P.; Van Tichelen, K.; Arien, B.; Vermeersch, F.; D'hondt, P.; Jongen, Y.; Ternier, S.; et al. MYRRHA: A multipurpose accelerator driven system for research & development. *Nuclear Instruments and Methods in Physics Research Section A: Accelerators, Spectrometers, Detectors and Associated Equipment* **2001**, *463*, 487−494.

(22) Abderrahim, H. A.; Baeten, P.; De Bruyn, D.; Fernandez, R. MYRRHA−A multi-purpose fast spectrum research reactor. *Energy Conversion and Management* **2012**, *63*, 4−10.

(23) Bandini, G.; Bubelis, E.; Schikorr, M.; Stempnievicz, M.; Tucek, K.; Lázaro, A.; Kudinov, P.; Kööp, K.; Jeltsov, M.; Mansani, L. Safety analysis results of representative DEC accidental transients for the ALFRED reactor. *International Conference on Fast Reactors and Related*

Fuel Cycles: Safe Technologies and Sustainable Scenarios (FR13); KTH Library, 2013.
(24) Alemberti, A.; Caramello, M.; Frignani, M.; Grasso, G.; Merli, F.; Morresi, G.; Tarantino, M. ALFRED reactor coolant system design. *Nucl. Eng. Des.* **2020**, *370*, 110884.
(25) Pelletier, M.; Guérin, Y. In *Comprehensive Nuclear Materials*, 2nd ed.; Konings, R., Ed.; Elsevier, 2020; Chapter 2.03, pp 72−105.
(26) Kleykamp, H. The chemical state of the fission products in oxide fuels. *J. Nucl. Mater.* **1985**, *131*, 221−246.
(27) Cappia, F.; Miller, B. D.; Aguiar, J. A.; He, L.; Murray, D. J.; Frickey, B. J.; Stanek, J. D.; Harp, J. Electron microscopy characterization of fast reactor MOX Joint Oxyde-Gaine (JOG). *J. Nucl. Mater.* **2020**, *531*, 151964.
(28) Plyushev, B.; Stepina, S.; Zimina, G.; Molchanova, O.; Savelyeva, L.; Yashkov, D. Melting diagrams of the binary systems MeI-SbI_3 and MeI-BiI_3 (Me-K, Rb, Cs). *Nonferrous Metallurgy* **1970**, *1*, 65−67.
(29) Dzeranova, K.; Kaloev, N.; Egerev, O.; Bukhalova, G. The BiI_3-CsI system phase diagram. *Zhurnal Neorganicheskoj Khimii* **1984**, *29*, 3171−3172.
(30) Kun, S.; Peresh, E. Y.; Lazarev, V. CsI-BiI_3 System and Homogeneity Ranges, Preparation, and Properties of $Rb_3(Cs_3)$-$Sb_2(Bi_2)I_9$ Single Crystals, CsBr-Bi(Sb)Br_3. *Neorganicheskie Materialy* **1988**, 1899−1903.
(31) Kaloev, N.; Kubalova, L.; Dzeranova, K.; Toporovskaya, E.; Paramazova, S. Thermodynamic Investigation of Binary BiI_3-RbI, BiI_3-CsI, and BiI_3-TII Systems in the Approximation of the Ideal Associated Solutions. *Russ. J. Inorg. Chem.* **1998**, *43*, 125−127.
(32) Lindqvist, O.; Johansson, G.; Sandberg, F.; Norin, T. Crystal structure of caesium bismuth iodide, $Cs_3Bi_2I_9$. *Acta Chem. Scand.* **1968**, *22*, 2943−2952.
(33) Sebastia-Luna, P.; Gélvez-Rueda, M. C.; Dreessen, C.; Sessolo, M.; Grozema, F. C.; Palazon, F.; Bolink, H. J. Potential and limitations of $CsBi_3I_{10}$ as a photovoltaic material. *Journal of Materials Chemistry A* **2020**, *8*, 15670−15674.
(34) Mel'Nikova, S.; Zaitsev, A. Ferroelectric phase transition in $Cs_3Bi_2I_9$. *Phys. Solid State* **1997**, *39*, 1652−1654.
(35) Melnikova, S.; Shabanova, L.; Zaitsev, A.; Parshikov, S.; Ageev, O.; Aleksandrov, K. Ferroelastic phase transition in $Cs_3Bi_2I_9$ crystal. *Ferroelectrics Letters Section* **1996**, *20*, 163−167.
(36) Arakcheeva, A.; Bonin, M.; Chapuis, G.; Zaitsev, A. The phases of $Cs_3Bi_2I_9$ between RT and 190 K. *Zeitschrift Für Kristallographie-Crystalline Materials* **1999**, *214*, 279−283.
(37) Arakcheeva, A.; Chapuis, G.; Meyer, M. The LT phase of $Cs_3Bi_2I_9$. *Zeitschrift für Kristallographie-Crystalline Materials* **2001**, *216*, 199−205.
(38) Gu, J.; Yan, G.; Lian, Y.; Mu, Q.; Jin, H.; Zhang, Z.; Deng, Z.; Peng, Y. Bandgap engineering of a lead-free defect perovskite $Cs_3Bi_2I_9$ through trivalent doping of Ru^{3+}. *RSC Adv.* **2018**, *8*, 25802−25807.
(39) McCall, K. M.; Stoumpos, C. C.; Kostina, S. S.; Kanatzidis, M. G.; Wessels, B. W. Strong electron-phonon coupling and self-trapped excitons in the defect halide perovskites $A_3M_2I_9$ (A= Cs, Rb; M= Bi, Sb). *Chem. Mater.* **2017**, *29*, 4129−4145.
(40) Tailor, N. K.; Satapathi, S. Crystalline-liquid duality of specific heat in halide perovskite semiconductor. *Scripta Materialia* **2023**, *223*, 115061.
(41) Filip, M. R.; Liu, X.; Miglio, A.; Hautier, G.; Giustino, F. Phase diagrams and stability of lead-free halide double perovskites $Cs_2BB'X_6$: B= Sb and Bi, B'= Cu, Ag, and Au, and X= Cl, Br, and I. *J. Phys. Chem. C* **2018**, *122*, 158−170.
(42) Ilyasov, I.; Chaurskii, N.; Barsegov, D.; Bergman, A. The adiagonal reciprocal system of caesium and lead chlorides and iodides. *Russ. J. Inorg. Chem.* **1967**, *12*, 1163−1165.
(43) Belyaev, I.; Shurginov, E.; Kudryashov, N. Thermographic Investigation of AI-BI_2 Binary Systems [A = K, Rb, or Cs and B = Cd, Hg, Sn or Pb. *Russ. J. Inorg. Chem.* **1972**, *17*, 1473−1475.
(44) Wells, H. L. Über die cäsium-und kalium-bleihalogenide. *Zeitschrift für anorganische Chemie* **1893**, *3*, 195−210.
(45) Møller, C. K. *On the Structure of Caesium Hexahalogeno-Plumbates (II)*; Munksgaard: Copenhagen, Denmark, 1960; Vol. 32.
(46) Wang, B.; Novendra, N.; Navrotsky, A. Energetics, structures, and phase transitions of cubic and orthorhombic cesium lead iodide ($CsPbI_3$) polymorphs. *J. Am. Chem. Soc.* **2019**, *141*, 14501−14504.
(47) Wang, B.; Navrotsky, A. Thermodynamics of cesium lead halide ($CsPbX_3$, X= I, Br, Cl) perovskites. *Thermochim. Acta* **2021**, *695*, 178813.
(48) Tsvetkov, D. S.; Mazurin, M. O.; Sereda, V. V.; Ivanov, I. L.; Malyshkin, D. A.; Zuev, A. Y. Formation thermodynamics, stability, and decomposition pathways of $CsPbX_3$ (X= Cl, Br, I) photovoltaic materials. *J. Phys. Chem. C* **2020**, *124*, 4252−4260.
(49) Sereda, V. V.; Sednev-Lugovets, A. L.; Malyshkin, D. A.; Tsvetkov, D. S.; Zuev, A. Y. High-temperature heat-flux inverse drop calorimeter. *Thermochim. Acta* **2020**, *694*, 178802.
(50) Dastidar, S.; Hawley, C. J.; Dillon, A. D.; Gutierrez-Perez, A. D.; Spanier, J. E.; Fafarman, A. T. Quantitative phase-change thermodynamics and metastability of perovskite-phase cesium lead iodide. *J. Phys. Chem. Lett.* **2017**, *8*, 1278−1282.
(51) Kye, Y.-H.; Yu, C.-J.; Kim, C.-H.; Kim, Y.-S.; Jong, U.-G. Influence of metal-ion replacement on the phase stabilization of cubic all-inorganic cesium lead halide perovskites: an ab initio thermodynamic formalism for solution-processed cation doping. *J. Phys. Chem. C* **2021**, *125*, 13195−13211.
(52) Evarestov, R.; Kotomin, E.; Senocrate, A.; Kremer, R.; Maier, J. First-principles comparative study of perfect and defective $CsPbX_3$ (X= Br, I) crystals. *Phys. Chem. Chem. Phys.* **2020**, *22*, 3914−3920.
(53) Zhang, B.; Zhang, H.; Lin, J.; Cheng, X. A time-dependent density functional study on optical response in all-inorganic lead-halide perovskite nanostructures. *Int. J. Quantum Chem.* **2020**, *120*, e26232.
(54) Li, M.; Peng, S.; Fang, S.; Gong, Y.; Yang, D.; Bu, K.; Liu, B.; Luo, H.; Guo, S.; Li, J.; et al. Synthesis of Two-Dimensional $CsPb_2X_5$ (X = Br and I) with a Stable Structure and Tunable Bandgap by $CsPbX_3$ Phase Separation. The. *J. Phys. Chem. Lett.* **2022**, *13*, 2555−2562.
(55) Dmitriev, Y. N.; Bennett, P.; Cirignano, L.; Gupta, T.; Klugerman, M.; Shah, K. Solid Solutions $(PbI_2)_x$−$(BiI_3)_{1-x}$. *MRS Online Proceedings Library (OPL)* **1999**, *580*, 99−104.
(56) Neuhausen, J.; Eichler, B. Investigations on the thermal release of iodine from liquid eutectic lead-bismuth alloy. *Radiochim. Acta* **2006**, *94*, 239−242.
(57) Zhang, J.; Yang, L.; Liu, R.; Chen, L. Stabilization of all-inorganic α-$CsPbI_3$ perovskite by Bi or Sb doping. *Materials Research Express* **2019**, *6*, 105529.
(58) Zhang, J.; Zhong, Y.; Chen, L.; Yang, L. Effect of B-site doping on the phase and thermal stability of $CsPbI_3$ perovskite. *Chem. Phys. Lett.* **2020**, *752*, 137572.
(59) Kajal, S.; Kim, J.; Shin, Y. S.; Singh, A. N.; Myung, C. W.; Kim, J. Y.; Kim, K. S. Unfolding the influence of metal doping on properties of $CsPbI_3$ perovskite. *Small Methods* **2020**, *4*, 2000296.
(60) Rietveld, H. M. A profile refinement method for nuclear and magnetic structures. *J. Appl. Crystallogr.* **1969**, *2*, 65−71.
(61) van Laar, B.; Schenk, H. The development of powder profile refinement at the Reactor Centre Netherlands at Petten. *Acta Crystallographica Section A: Foundations and Advances* **2018**, *74*, 88−92.
(62) Le Bail, A.; Duroy, H.; Fourquet, J. Ab-initio structure determination of $LiSbWO_6$ by X-ray powder diffraction. *Mater. Res. Bull.* **1988**, *23*, 447−452.
(63) Rodríguez-Carvajal, J. Recent advances in magnetic structure determination by neutron powder diffraction. *Physica B: Condensed Matter* **1993**, *192*, 55−69.
(64) Höhne, G.; Cammenga, H.; Eysel, W.; Gmelin, E.; Hemminger, W. The temperature calibration of scanning calorimeters. *Thermochim. Acta* **1990**, *160*, 1−12.
(65) Beneš, O.; Konings, R.; Wurzer, S.; Sierig, M.; Dockendorf, A. A DSC study of the $NaNO_3$-KNO_3 system using an innovative encapsulation technique. *Thermochim. Acta* **2010**, *509*, 62−66.

https://doi.org/10.1021/acs.jpcc.3c02696
J. Phys. Chem. C 2023, 127, 17482−17496

(66) Boettinger, W. J.; Kattner, U. R.; Moon, K.-W.; Perepezko, J. H. In *Methods for Phase Diagram Determination*; Zhao, J.-C., Ed.; Elsevier Science Ltd: Oxford, 2007; pp 151−221.
(67) Lukas, H. L.; Fries, S. G.; Sundman, B. *Computational Thermodynamics: the Calphad method*; Cambridge University Press, 2007; Vol. *131*.
(68) Centre for Research in Computational Thermochemistry, FactSage 8.2. 20222; http://www.factsage.com, Date of last access: June 9, 2023.
(69) Capelli, E.; Beneš, O.; Konings, R. Thermodynamics of soluble fission products cesium and iodine in the Molten Salt Reactor. *J. Nucl. Mater.* **2018**, *501*, 238−252.
(70) Chase, M. W. *NIST-JANAF Thermochemical Tables*; American Chemical Society: Washington, DC, 1998; Vol. *9*.
(71) Konings, R.; Cordfunke, E.; van der Laan, R. Enthalpy increment measurements of PbI_2: evidence for a reversible polytypic transition. *J. Alloys Compd.* **1995**, *230*, 85−88.
(72) Cubicciotti, D. Enthalpy of Formation of bismuth (III) Iodide and the Dissociation Energy of bismuth (I) Iodide. *Inorg. Chem.* **1968**, *7*, 211−213.
(73) Barin, I.; Knacke, O.; Kubaschewski, O. *Thermochemical properties of inorganic substances*; Springer, 1977; pp 1−861.
(74) Cubicciotti, D.; Eding, H. The Thermodynamic Functions above Room Temperature for Antimony and Bismuth Iodides and Their Absolute Entropies. *J. Phys. Chem.* **1965**, *69*, 3621−3625.
(75) Neumann, F. Investigation of Specific Heat of Minerals. *Ann. Phys. Chem.(Poggendorff)* **1831**, *99*, 1−39.
(76) Kopp, H., III XX.-Investigations of the specific heat of solid bodies. *Philosophical Transactions of the Royal Society of London* **1866**, *19*, 154−234.
(77) Pelton, A. D.; Chartrand, P.; Eriksson, G. The modified quasi-chemical model: Part IV. Two-sublattice quadruplet approximation. *Metallurgical and Materials Transactions A* **2001**, *32*, 1409−1416.
(78) Pelton, A. D. A general "geometric" thermodynamic model for multicomponent solutions. *Calphad* **2001**, *25*, 319−328.
(79) Sundman, B.; Lukas, H.; Fries, S. *Computational thermodynamics: the Calphad method*; Cambridge University Press: Cambridge, 2007.
(80) Trots, D.; Myagkota, S. High-temperature structural evolution of caesium and rubidium triiodoplumbates. *J. Phys. Chem. Solids* **2008**, *69*, 2520−2526.
(81) Fazio, C.; Sobolev, V.; Aerts, A.; Gavrilov, S.; Lambrinou, K.; Schuurmans, P.; Gessi, A.; Agostini, P.; Ciampichetti, A.; Martinelli, L.; et al. *Handbook on lead-bismuth eutectic alloy and lead properties, materials compatibility, thermal-hydraulics and technologies*, 2015 ed.; Nuclear Energy Agency/Organisation for Economic Co-Operation and Development, 2015; pp 70−78.
(82) Cordfunke, E.; Prins, G. The thermochemical properties of caesium iodide. I. Thermodynamic functions of solid CsI. *Thermochim. Acta* **1985**, *90*, 169−176.
(83) Roki, F.-Z.; Ohnet, M.-N.; Fillet, S.; Chatillon, C.; Nuta, I. Critical assessment of thermodynamic properties of CsI solid, liquid and gas phases. *J. Chem. Thermodyn.* **2014**, *70*, 46−72.
(84) Marronnier, A.; Roma, G.; Boyer-Richard, S.; Pedesseau, L.; Jancu, J.-M.; Bonnassieux, Y.; Katan, C.; Stoumpos, C. C.; Kanatzidis, M. G.; Even, J. Anharmonicity and disorder in the black phases of cesium lead iodide used for stable inorganic perovskite solar cells. *ACS Nano* **2018**, *12*, 3477−3486.
(85) Degen, T.; Sadki, M.; Bron, E.; König, U.; Nénert, G. The highscore suite. *Powder Diffraction* **2014**, *29*, S13−S18.

https://doi.org/10.1021/acs.jpcc.3c02696
J. Phys. Chem. C 2023, 127, 17482−17496